Applied Energy 255 (2019) 113836

Contents lists available at ScienceDirect

Applied Energy

journal homepage: www.elsevier.com/locate/apenergy

Thermal performance and economic analysis of supercritical Carbon Dioxide cycles in combined cycle power plant

Dhinesh Thanganadar, Faisal Asfand, Kumar Patchigolla*

School of Water, Energy and Environment (SWEE), Cranfield University, Cranfield MK43 0AL, UK

HIGHLIGHTS

- Identified the optimal GT pressure ratio requirements for four sCO_2 cascaded cycles.
- Pressure ratio of a sCO_2 cycle at maximum efficiency is higher than a steam cycle.
- Multi-objective optimisation is done to compare sCO_2 cycles on equivalent basis.
- Performance prediction maps were produced to help selecting an optimal GT.
- A new sCO_2 cycle is proposed that improves efficiency by 1.4 percentage points.

ARTICLE INFO

Keywords:
Supercritical CO_2 cycle
Gas turbine
Combined cycle
Multi-objective optimisation
Optimum pressure ratio
sCO_2

ABSTRACT

A closed-loop, indirect, supercritical Carbon Dioxide (sCO_2) power cycle is attractive for fossil-fuel, solar thermal and nuclear applications owing to its ability to achieve higher efficiency, and compactness. Commercial Gas Turbines (GT's) are optimised to yield maximum performance with a conventional steam Rankine cycle. In order to explore the full potential of a sCO_2 cycle the whole plant performance needs to be considered. This study analyses the maximum performance and cost of electricity for five sCO_2 cascaded cycles. The plant performance is improved when the GT pressure ratio is considered as a design variable to a GT to optimise the whole plant performance. Results also indicate that each sCO_2 Brayton cycle considered, attained maximum plant efficiency at a different GT pressure ratio. The optimum GT pressure ratio to realise the maximum cost reduction in sCO_2 cycle was higher than the equivalent steam Rankine cycle. Performance maps were developed for four high efficient cascaded sCO_2 cycles to estimate the specific power and net efficiency as a function of GT turbine inlet temperature and pressure ratio. The result of multi-objective optimisation in the thermal and cost (c$/kWh) domains and the Pareto fronts of the different sCO_2 cycles are presented and compared. A novel sCO_2 cycle configuration is proposed that provides ideal-temperature glide at the bottoming cycle heat exchangers and the efficiency of this cycle, integrated with a commercial SGT5-4000F machine in lieu of a triple-pressure steam Rankine cycle, is higher by 1.4 percentage point.

1. Introduction

The UK is committed to reducing greenhouse gas emissions by at least 80% of 1990 levels by 2050 [1]. Meeting such a rigorous carbon emission reduction goal requires significant technological breakthroughs in the power generation industries. Although post-combustion carbon capture technologies are technically feasible, it is not economically attractive to implement in coal-fired power plants owing to a penalty in the net efficiency of about 7.7–11.9% points [2]. Hence new thermodynamic cycles that enhance CO_2 capture will become more practical if they can produce power at higher efficiency compared to conventional power technologies. sCO_2 cycles are therefore gaining more attention. The Supercritical Carbon Dioxide (sCO_2) Brayton cycle has many advantages over the conventional steam Rankine cycle or Brayton cycle owing to its simple layout, higher efficiency, and compact equipment size. The sCO_2 Brayton cycle is considered suitable for different heat sources such as nuclear, solar thermal, and fossil-fuel. A commercial packaged unit is currently available for low-grade waste heat recovery (WHR) applications from Echogen [3]. Although several research studies have been done in the context of integrating an sCO_2 Brayton cycle with nuclear and solar applications [4,5] limited attention has been given to cycle optimisation. The National Renewable

* Corresponding author.
E-mail address: k.patchigolla@cranfield.ac.uk (K. Patchigolla).

https://doi.org/10.1016/j.apenergy.2019.113836
Received 28 June 2019; Received in revised form 20 August 2019; Accepted 1 September 2019

Nomenclature

CCPP	Combined Cycle Power Plant
COE	Cost of Electricity
GT	Gas Turbine
HRSG	Heat Recovery Steam Generator
HT	High Temperature
HTR	High Temperature Recuperator
LMTD	Log Mean Temperature Difference
LT	Low Temperature
LTR	Low Temperature Recuperator
MT	Medium Temperature
NSGA	Non-dominated Sorting Genetic Algorithm
ORC	Organic Rankine Cycle
PR	Pressure ratio
RRC	Recuperated Recompression Cycle
sCO_2	Supercritical Carbon dioxide
SRBC	Simple Recuperative Brayton Cycle
TET	Turbine Exhaust Temperature
TIT	Turbine Inlet Temperature
WHR	Waste Heat Recovery

Energy Laboratory (NREL) is setting up a small scale plant of 10 MW_e capacity after the successful demonstration of a pilot plant having 520 kW_{th} of heater power [6]. Electric Power and Research Institute (EPRI), Institute of Advanced Engineering (IAE) [7], Électricité de France (EDF) and Echogen are leading research on developing an advanced indirect sCO_2 Brayton cycle integrated with a coal-fired power plant [8] whilst NET power is currently testing an oxy-combustion direct-fired sCO_2 Brayton cycle [9].

Crespi et al. [10] presented a review of forty-two sCO_2 cycles for power generation application and categorised them. Zhao et al. [11] proposed a novel cycle configuration that utilises heat from syngas and an oxygen compressor with multi-stream recuperators in a direct-fired sCO_2 cycle using syngas from coal gasification, yielding 43.7% net efficiency on an LHV basis. Heo et al. [12] performed a thermodynamic study on iso-thermal compression for WHR which identified performance improvement potential. This study showed that ~50% of the compression work can be reduced in the sCO_2 cycle by using iso-thermal compression when the inlet pressure is fixed at 74 bar. Wang et al. [13] demonstrated the performance of transcritical CO_2 (tCO_2) cycle and Organic Rankine Cycle (ORC) for different fluids such as R123, R245fa, toluene, isobutane, isopentane and cyclohexane to recover the low-grade heat from a recompression supercritical CO_2 cycle before the precooler using exergo-economic analysis. They concluded that the performance of tCO_2 cycles is better for lower sCO_2 cycle pressure ratios and the ORC cost is slightly lower than tCO_2 cycles. Baik et al. [14] on the other hand, compared tCO_2 cycles with a transcritical R125 (t-R125) cycle for low-grade WHR (100 °C) application concluding that t-R125 cycle produces about 14% more power than a tCO_2 cycle.

The sCO_2 cycle pressure ratio is lower relative to a steam Rankine cycle and also the isobaric specific heat capacity (C_p) of sCO_2 is 2–4 times lower than that of steam on a mass basis over the temperature range of interest. Hence the sCO_2 mass flow is 8–12 times higher than the steam mass flow at the same thermal input [15]. Moreover, the C_p is highly variable due to the occurrence of a pseudo-critical condition and therefore the capacitance (the product of mass flow and isobaric specific heat) of the sCO_2 stream changes significantly as a function of pressure and temperature, which limits the maximum possible heat extraction from the flue gas side with a single heat exchanger (or a single sCO_2 mass flow) because of the pinch point. The C_p of sCO_2 shown in Fig. 1 clearly shows that, with a single mass flow, the high-pressure sCO_2 stream can extract the heat from a GT exhaust flue gas heat between ~600 °C and ~300 °C with high exergetic efficiency. The increase in sCO_2 isobaric specific heat at a lower temperature (< 300 °C) requires a reduction in sCO_2 flow rate to match the stream capacitances to obtain further heat extraction whilst avoiding a pinch point. Therefore the heat extraction has to be split in order to maximise the energy transfer with a higher second law efficiency, making cascade cycles attractive options.

Khadse et al. [16] performed an optimisation study for a Simple Recuperative Brayton Cycle (SRBC) and Recuperated Recompression Cycles (RRC) to recover the waste heat from a GT exhaust concluding that using an sCO_2 cycle as the bottoming cycle in lieu of a conventional steam Rankine cycle reduces cost by ~28%. Khadse et al. [17] also performed an optimisation and highlighted that the sCO_2 turbine inlet temperature tends to reach the lower boundary in the search space when maximising the net power produced from WHR as the main heat exchanger pinch point is the limiting parameter. Marchionni et al. [18] compared the thermal and economic performance of eight sCO_2 cycles for WHR applications for TIT 250–600 °C and concluded that the SRBC was economically attractive for small-scale WHR applications. Kimzey [19] compared the standard higher efficienct sCO_2 cycles such as SRBC, RCBC finding that, although these cycles can yield higher efficiency for constant heat flux heat sources, it is not attractive for sensible heat sources but cascade cycles performed better. Cho et al. [20] studied recompression with partial heating cycle, precompression cycle with partial heating cycle and three cascade cycles proposed in Kimzey [19] as a bottoming cycle solution for SGT5-4000F GT exhaust conditions. This study concluded that cascade cycle 2 and cascade cycle 3 performance were superior to the other cycles studied and the plant efficiency increased by 0.7%pts with cascade cycle 3 over the steam cycle. Integration of the bottoming cycle is highly sensitive to the quality of flue gas from the GT exhaust [16] which indicates that different sCO_2 cycles can be attractive for a different exhaust gas temperatures. Wright et al. [21] performed an economic study of SRBC, cascade cycle, dual recuperative cycle and preheating cycle finding that although the efficiency of the cascaded and preheating cycle was higher the unit capacity cost ($/$kW_e$) was also higher than the other cycles.

Despite having a high-temperature difference across the primary heat exchanger, the partial cooling cycle [22] limits the potential to achieve high efficiency because the single flue gas heat exchanger in the partial cooling cycle and the initial results show that the modified

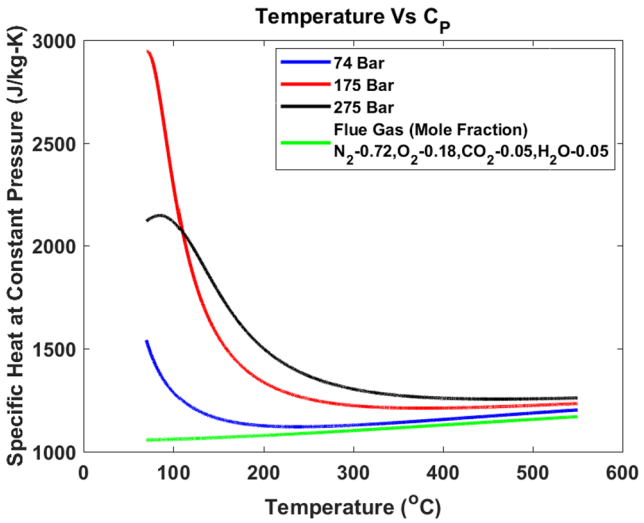

Fig. 1. Isobaric specific heat variation as a function of Temperature for three different pressures of sCO_2 and a typical flue gas.

layouts with an anabranch from the compressor for partial heating didn't offer comparable performance to the cascade cycles. In a nutshell, it can also be concluded that the SRBC and RCBC cycles can't extract maximum heat from the flue gas with higher exergic efficiency as they use one primary heat exchanger with a single sCO_2 mass flow, therefore, this study focused on high-efficient cascade cycles as a bottoming cycle solution. Held et al. [22] proposed a dual-rail cycle (designated as cascade cycle#4 in this paper), which is an extension of the cycle described as cascade 3 in this paper, which offers an ideal temperature glide between the two streams of the exhaust heat exchanger because of the additional degrees of freedom. It should be noted that this perfect capacitance match in a Heat Recovery Steam Generator (HRSG) is limited, even after having three pressure stages in a conventional steam Rankine cycle, owing to the evaporator (latent heat transfer process). That study considered six different capacity GT's, from small to heavy-duty machines and confirmed that the trend in cost-saving potential with increasing GT capacity remains valid for that sCO_2 cycle. Huck et al. [23] performed an exergic study of the sCO_2 cycle for higher temperature exhaust gas (~700 °C) for next-generation bottoming cycle for CCPP (> 63% net efficiency) and concluding that exergy destruction is higher, and accordingly, performance is lower for a sCO_2 cycle than a triple-pressure HRSG.

The thermal performance of a Gas Turbine (GT) is highly influenced by the air compressor pressure ratio and GT Turbine Inlet Temperature (TIT). For a given GT TIT the pressure ratio that maximises GT net efficiency is higher than the pressure ratio that maximises GT specific power. Specific power is an important parameter for a GT as a higher value allows a smaller size of GT to produce the same output power. Davidson and Keeley [24] highlighted that the optimum GT pressure ratio selection has to minimise the major heat losses (in a conventional steam-based CCPP occur at the HRSG and the steam condenser) which generally translates to maximising the output power fraction of the topping cycle (analogues to GT specific power). Maximising the GT specific power is contrary to maximising the GT efficiency as maximising GT specific power tends to increase the net power generation of the higher cycle (topping cycle) which eventually increases the fuel flow to the combustor. In order to increase the fuel flow to the combustor for a given GT firing temperature, the combustor inlet air temperature should be lower and this implies a lower pressure ratio. Maximising the efficiency, on the other hand, tends to increase the pressure ratio in order to minimise the fuel flow to the combustor up to the level of economic compression. Cerri [25] highlighted that the optimum pressure ratio of a GT in CCPP is intermediate between those for which the efficiency and GT specific power are maximum. Horlock [26] also compared the optimal pressure ratio for dry and humid cycles. Najjar and Ismail [27] analysed the impact of operating parameters in the optimal pressure ratio and the study concludes that the pressure ratio corresponds to maximum GT specific power is more sensitive than those for which efficiency is maximum. The CC specific power reaches a maximum at a lower pressure ratio than that corresponding to the maximum GT specific power, due to the utilisation of exhaust heat by the bottoming cycle. Previous studies on conventional CCPP also showed that increasing GT firing temperature also increases the optimal pressure ratio of a GT [24]. Moreover, the optimal GT pressure ratio can vary as the isentropic efficiencies of the air compressor and GT change [27].

Previous studies have analysed the performance of different sCO_2 Brayton cycles for only a single, commercially available, GT exhaust condition. However, this methodology doesn't guarantee to yield maximum performance of sCO_2 Brayton cycles as commercially available GT's are optimised to yield maximum performance when coupled with a bottoming steam Rankine cycle [15]. Also, that does not identify whether underperformance of one sCO_2 cycle at a single GT exhaust condition can be generalised to different GT exhaust conditions. In order to access the complete design space of a sCO_2 Brayton cycle for bottoming cycle applications, the whole plant model has to be either optimised to maximise both plant efficiency and net power or minimise the total cost in combination with the GT. This paper introduces a general concept for integrating sCO_2 cycles with Combined Cycle Power Plant (CCPP) and also demonstrates the maximum potential of sCO_2 cycles without being limited to any commercially available GT. Four different cycles, named the cascade cycle#2, the cascade cycle#3 [20], and cycle 4 were presented by Held et al. [22] and a novel cascade cycle (designated as cascade cycle#5 in this paper) are analysed as a bottoming cycle solution and multi-objective optimisation is performed to compare the Pareto front for different cycles on an equivalent basis in view of whole plant thermal performance and cost. The optimal pressure ratio requirement of GT air compressor to yield maximum efficiency of an integrated sCO_2-combined cycle power plant is compared with the pressure ratio which will provide

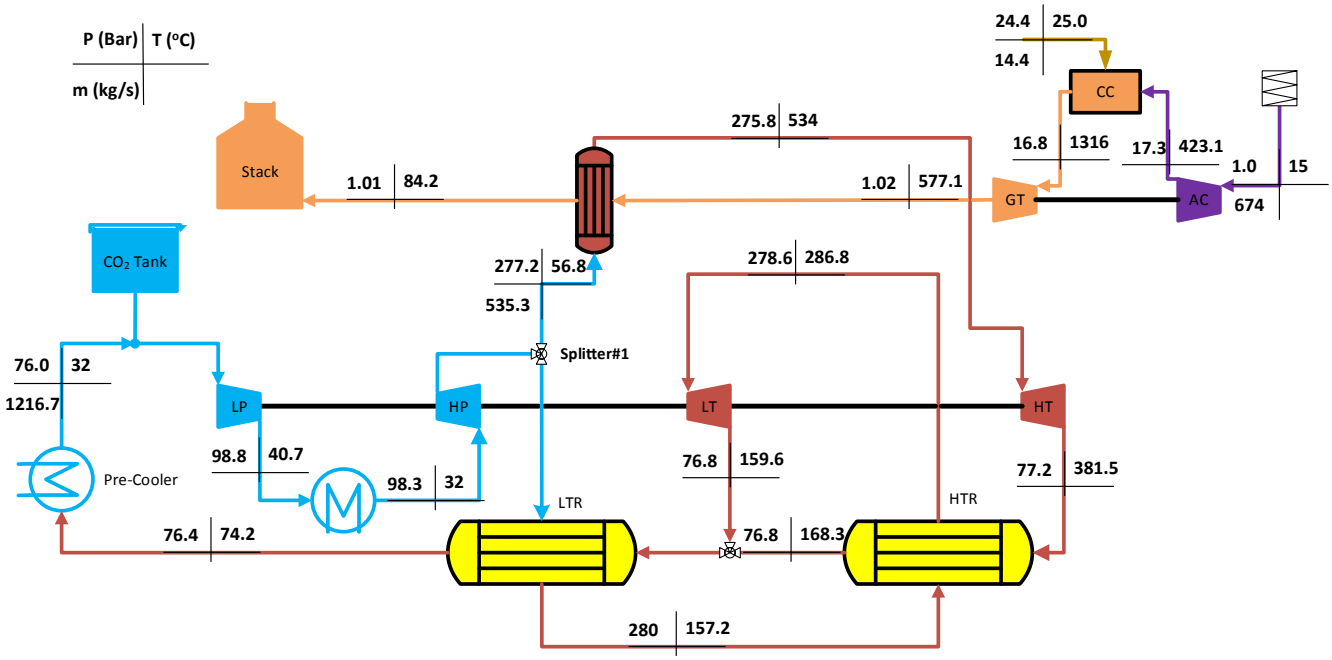

Fig. 2. Cascade Cycle 1 Configuration (Cycle 1).

maximum GT specific power. Since commercial GT pressure ratio is fixed, set of performance maps for all the four sCO_2 cycles were developed, which helps to estimate the performance of sCO_2 cycles for a given GT pressure ratio and TIT.

2. Supercritical CO_2 cycle configurations

The isobaric specific heat of sCO_2 varies widely with the temperature, as shown in Fig. 1 for three different pressure levels, due to the occurrence of a pseudo-critical state. It can be clearly seen that the C_p at low-temperature is roughly twice the C_p at higher-temperature. The typical GT exhaust gas temperature of a heavy-duty GT is about 500–620 °C (this range is broader for aero-derivative engines) and this exhaust gas temperature has to be cooled down to ~70 to 150 °C. The minimum exhaust stack temperature is dictated by the conversion of sulphur from the fuel into SO_3 that reacts with moisture and forms sulphuric acid, which condenses and corrodes the tube material if the local tube metal temperature is lower than the dew point temperature. Since the UK and many other countries are moving towards utilising natural gas as the fuel in the near future, or fuel with low sulphur content, the exhaust stack temperature can go below 100 °C. To utilise the maximum heat energy from flue gas within this window of ~600 to 100 °C with a heat exchanger that operates with a single mass flow will trade-off its outlet sCO_2 temperature. Maximising the cycle net efficiency will also ensure maximum net power output of the cycle whilst simulating both topping and bottoming cycle (Eq. (1)) as opposed to modelling only the bottoming cycle where the net energy transfer has to be maximised. In the latter case, maximising the efficiency will lower the waste heat recovery from the flue gas (minimising the denominator in Eq. (2)) [19].

$$\eta_{cycle,net} = \frac{W_{GT,net} + W_{ST,net}}{m_{fuel} * LHV} \quad (1)$$

$$\eta_{bottom,net} = \frac{W_{ST,net}}{Q_{in} - Q_{stack}} \quad (2)$$

2.1. Cascade Cycle 1

The integrated cascade Brayton cycle configuration with the commercial SGT5-4000F is shown in Fig. 2 and the Temperature-Entropy (TS) diagram is shown in Fig. 3. The layout is optimised to maximise the overall cycle net efficiency by changing the sCO_2 mass flow, high and low-pressure levels of the sCO_2 cycle, splitter #1 fraction, and sCO_2 compressor intercooler upstream pressure. The splitter finds the optimal position to maximise the heat extraction from both flue gas heater and recuperators. This configuration has only one flue gas heat exchanger and the UA of the heat exchanger is relatively low owing to higher LMTD hence the cost of the heat exchanger might potentially be lower than other cycles. Therefore, this cycle becomes attractive where the efficiency becomes less significant such as lower capacity WHR applications due to its simple layout compared to other cascade cycles. The Temperature-Heat Transfer (T-Q) diagram is shown in Fig. 4 which shows that the heat transfer is limited by the pinch at the inlet of the LT Recuperator (LTR) and as a consequence, heat transfer is a trade-off with sCO_2 turbine inlet temperatures.

2.2. Cascade Cycle 2

The integrated cascade Brayton Cycle 2 configuration with the commercial SGT5-4000F machine is shown in Fig. 5 and the TS diagram is shown in Fig. 6. The layout is optimised to maximise the cycle net efficiency by optimising the same parameters considered for Cycle 1. Whilst performing the optimisation to maximise the overall cycle net efficiency, the splitter fraction is optimised so that maximum heat can be transferred from the exhaust flue gas heater and the recuperators with higher exergetic efficiency. This fraction will be the critical control parameter to ensure maximum cycle efficiency and therefore it has to be re-optimised for every design or change in operating parameter, e.g. ambient temperature. This cycle does not have the full flexibility of matching the capacitance of hot and cold streams in the LTR and HT Recuperator (HTR), and exhaust heat exchangers owing to the highly varying specific heat of sCO_2 as a function of pressure and temperature. Hence the heat exchanger minimum pinch point will decide the optimal size of the heat exchanger and that in turn will control the plant cost. A trade-off has to be made between higher efficiency and cost, as a smaller pinch increases the cost exponentially. This study considers a minimum pinch point of 3 °C. The optimum design maximises the energy transfer in the recuperator and exhaust heat exchanger by matching the capacitance of both LTR and LT flue gas with the trade-off in exergetic efficiency of HTR and HT flue gas heater as shown in Fig. 7.

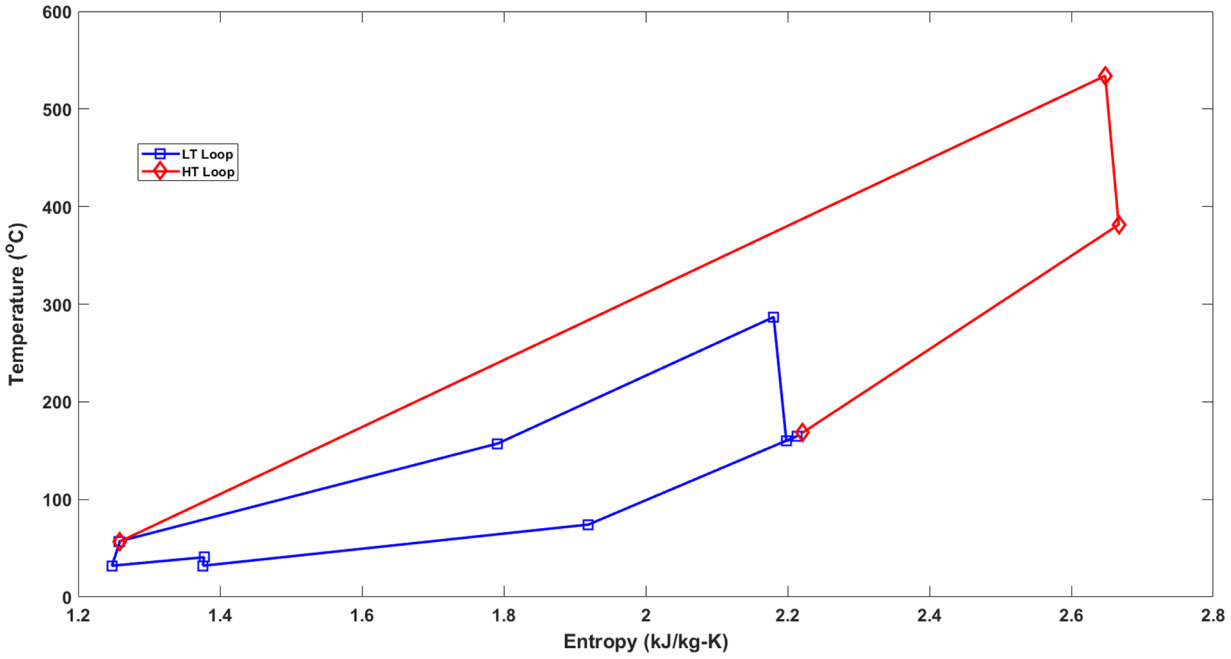

Fig. 3. Cascade Cycle 1: TS Diagram.

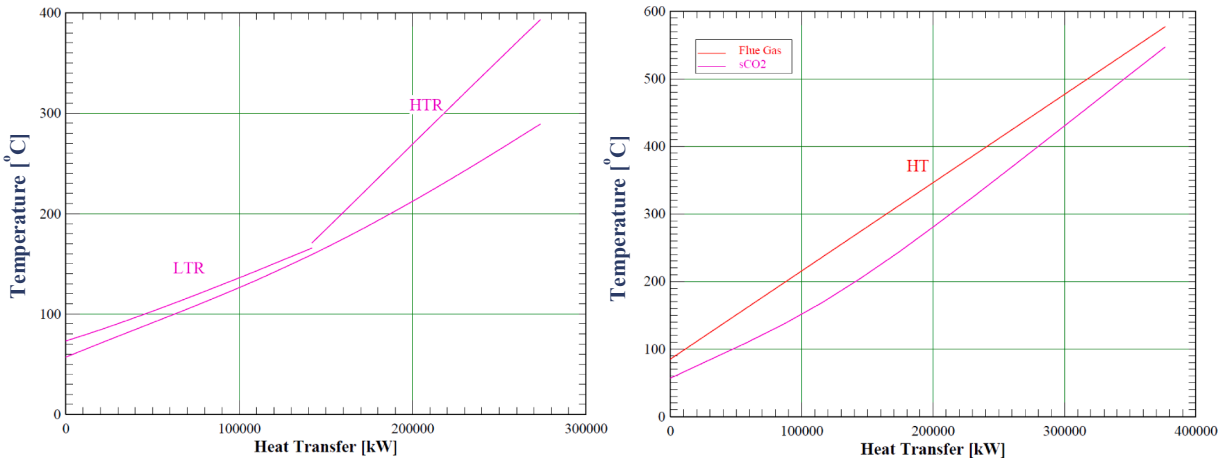

Fig. 4. T-Q Diagram of Cascade Cycle 1: Left- Recuperators, Right- Flue gas Heat exchanger.

2.3. Cascade Cycle 3

Cycle 3 is an adaptation of Cycle 2 in order to improve the overall efficiency of the cycle by changing the configuration as shown in Fig. 8. The TS diagram of Cycle 3 is shown in Fig. 9. Splitter 2 adds another degree of freedom to control the flow requirement between the HTR and HT flue gas heat exchanger. This configuration ensures maximum energy transfer in the exhaust gas heat exchangers and recuperator. The optimal cycle results in lower exergetic efficiency in the HTR as shown in Fig. 10.

2.4. Cascade Cycle 4

In order to improve the efficiency further, Echogen proposed a cycle named "Dual-rail" cycle (in this paper this cycle is designated as Cycle 4) which is the modified version of Cycle 3 [22]. This new cycle mixes an anabranch from the outlet of the HTR cold stream that mixes with the outlet of the MT flue gas heat exchanger and supplies a higher mass flow to the HT flue gas heat exchanger as shown in Fig. 11. The TS diagram of Cycle 4 is shown in Fig. 12. It can be seen from Fig. 1 that the mass flow of sCO_2 to the exhaust gas heat exchanger as has to be increased to accommodate the change in specific heat from low temperature to a high temperature so that the slope of the dropping temperature profile can be matched. The cycle pressure ratio fixes the outlet temperature of the HT sCO_2 turbine and this fixes the cold stream outlet temperature of the HTR outlet temperature by the decided minimum approach temperature. This becomes the inlet to the LT sCO_2 turbine. The decision as to the optimum value of sCO_2 mass flow to the HT exhaust gas heater is the trade-off between maximising the exergetic efficiency and maximising the heat transfer as the pinch occurs at the cold end of the HT flue gas heater (owing to higher isobaric heat capacity at lower temperature), and this leads to ~50 °C lower approach temperature for the SGT5-4000F machine exhaust conditions as shown in Fig. 13. It is worth noting that the conventional steam Rankine cycle cannot have this perfect temperature matching, i.e. 'ideal temperature gliding' owing to the occurrence of a phase-change which might shift the pinch point to the outlet of the evaporator.

2.5. Cascade Cycle 5

The difference in temperature at the HT flue gas heater can be further minimised with the layout proposed in Fig. 14 and the corresponding TS

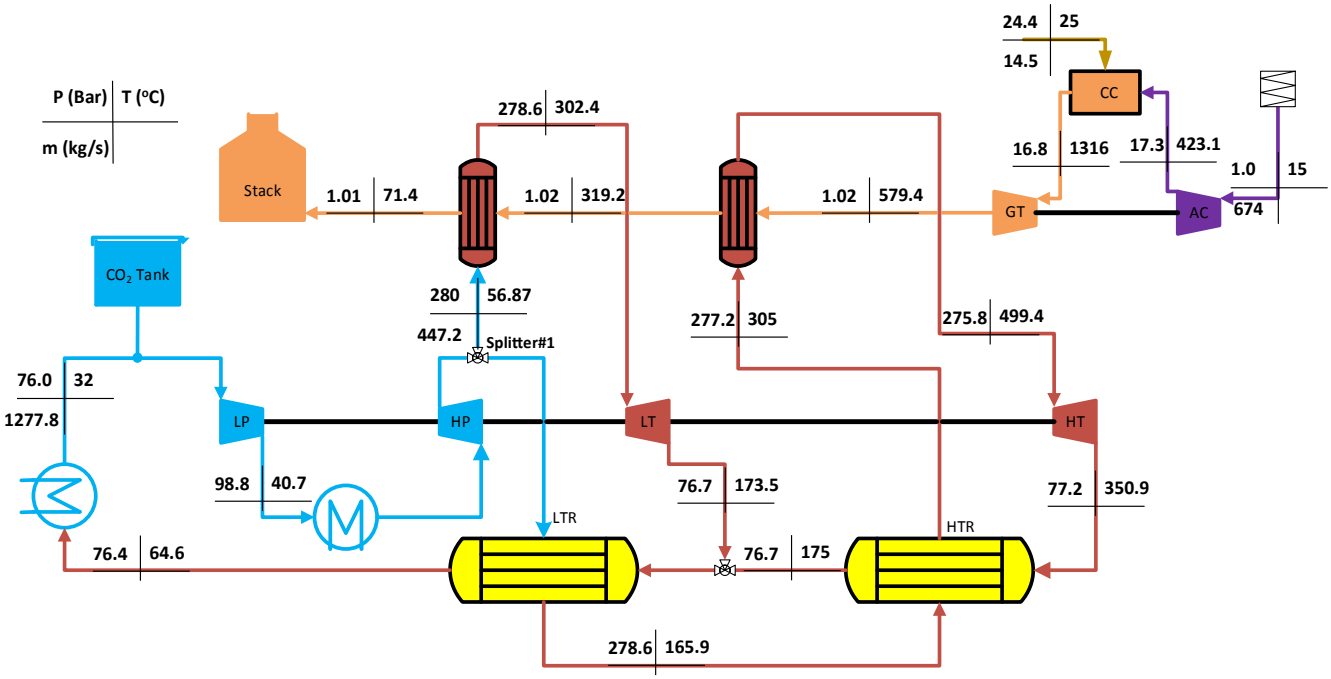

Fig. 5. Cascade Cycle 2 Configuration (Cycle 2).

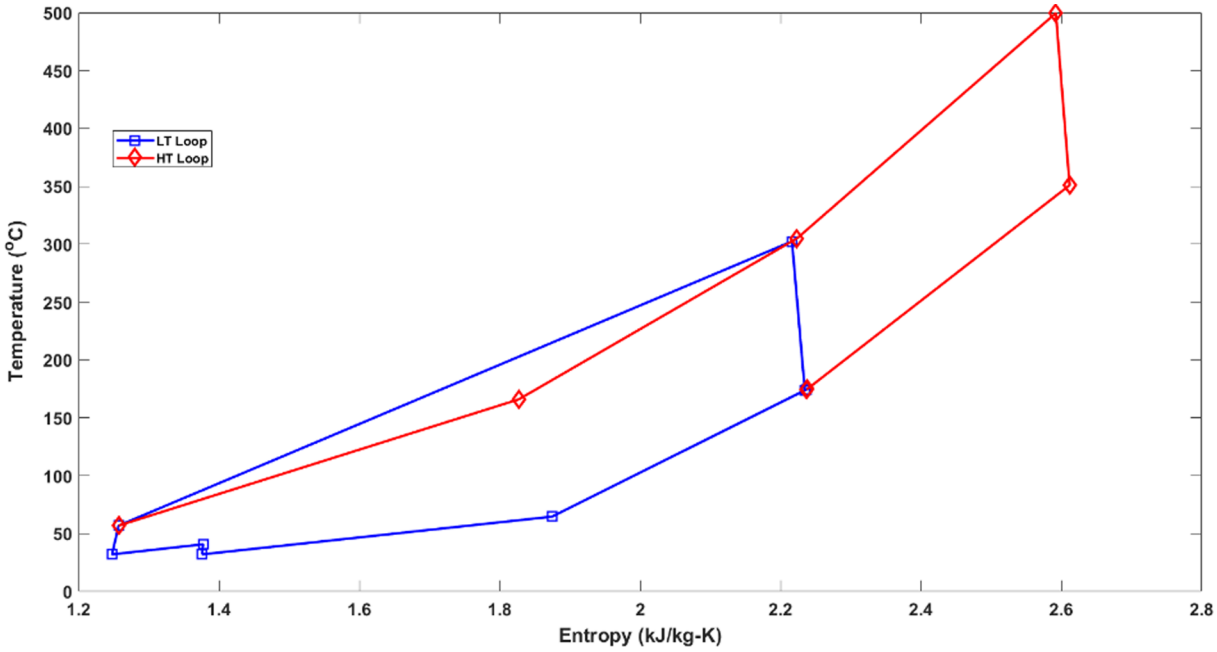

Fig. 6. Cascade Cycle 2: TS Diagram.

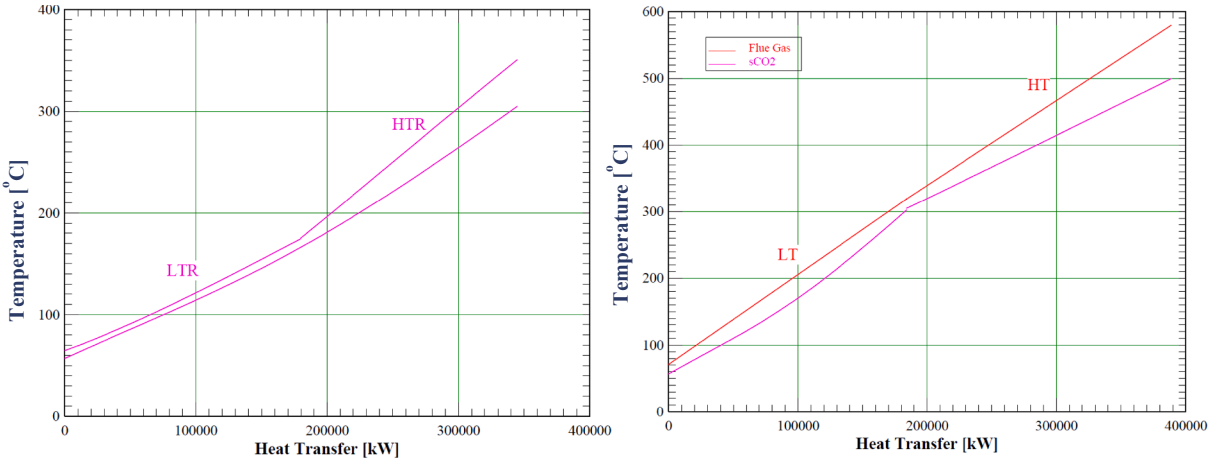

Fig. 7. T-Q Diagram of Cascade Cycle 2: Left- Recuperators, Right- Flue gas Heat exchanger.

diagram is shown in Fig. 15. This cycle adds another degree of freedom to the cycle by integrating an exhaust gas heat exchanger, splitter, recuperator and a turbine. This modification has the full flexibility to control the mass flow to maximise energy transfer with higher exergic efficiency which matches the slope of hot and cold fluid temperature change in both recuperators and exhaust heat exchangers as shown in Fig. 16, and therefore improves the net efficiency further. Although this cycle offers the maximum net efficiency, the improvement in performance is not significant for its increased complexity, therefore, the Cost of Electricity (COE) can be higher. From Fig. 16, it is clear that the hot stream follows well with the cold stream that will make the UA higher than other cycles owing to a lower LMTD. This may further increase the COE. However, this cycle can be attractive when the GT exhaust gas temperature is higher in order to better match the larger variation of sCO_2 Cp with lesser exergy destruction in the exhaust gas heat exchangers.

3. Methodology

The thermodynamic cycles were simulated for an SGT5-4000F turbine to benchmark with results by Cho et al. [20]. In order to investigate the maximum cycle net efficiency and minimum cost whilst integrating sCO_2 cycles with a different scale of GT's, both the GT and the sCO_2 cycle has been modelled. The main design variables for different sizes of GT in the topping cycle were the pressure ratio and the GT inlet temperature, compressor inlet air mass flow, pressure drop, cooling flow fraction and the turbomachinery isentropic efficiency. In this study, only the compressor pressure ratio and GT TIT are considered as variables whilst the air mass flow, the turbomachinery isentropic efficiency and the pressure drop at air intake/ combustors were kept constant in the optimization study. The GT and Combined Cycle (CC) specific power (kJ/kg) are calculated using Eq. (3). Note the air mass flowrate is considered for specific power calculation and net efficiency is reported in this paper unless otherwise specified.

$$SP_{GT} = \frac{W_{GT,net}}{\dot{m}_{air}};\ SP_{CC} = \frac{W_{GT,net} + W_{sCO_2\ \ Turbine,net}}{\dot{m}_{air}} \tag{3}$$

3.1. Model assumptions and input conditions

A thermodynamic process model was developed in Thermoflex, a commercial heat and mass balance software, which uses the REFPROP

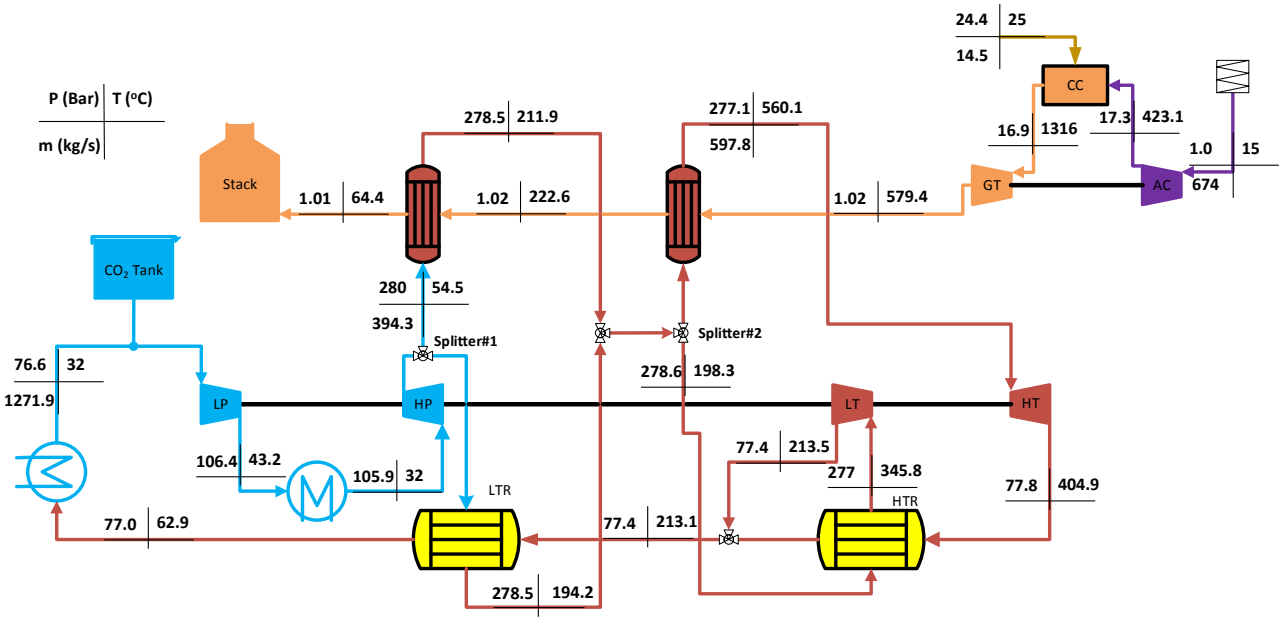

Fig. 8. Cascade Cycle 3 Configuration (Cycle 3).

fluid property database developed by the National Institute of Standards and Technology (NIST) [28], which is the most accurate equation of state available to predict sCO_2 thermodynamic properties [29]. REFPROP uses the Span-Wagner Equation of State (EoS) to calculate the properties of the pure components [30]. The cycles are modelled at ISO ambient condition and no lower limit in stack temperature is imposed. The piping pressure loss and heat loss to the ambient are neglected in this study. Table 1 shows the thermodynamic model assumptions considered for this study.

Thermoflex solves the steady-state heat and mass balance for all the components.

The component mass balance of a component is calculated by Eq. (4),

$$\sum \dot{m}_{in} = \sum \dot{m}_{out} \tag{4}$$

The energy balance of a component is calculated by Eq. (5),

$$\sum \dot{m}_{in} * h_{in} - \sum \dot{m}_{out} * h_{out} + \sum Q + W = 0 \tag{5}$$

where $\dot{m}$ is the mass flow rate, Q is the heat flows, W is the shaft work and h is the enthalpy.

The air compressor of GT is modelled using polytropic efficiency as an input and the outlet temperature is calculated using Eq. (6),

$$T_o = T_i * \left(\left(\frac{P_o}{P_i} \right)^{\frac{R}{c_p * \eta_p}} \right) \tag{6}$$

The GT outlet temperature can be calculated using Eq. (7),

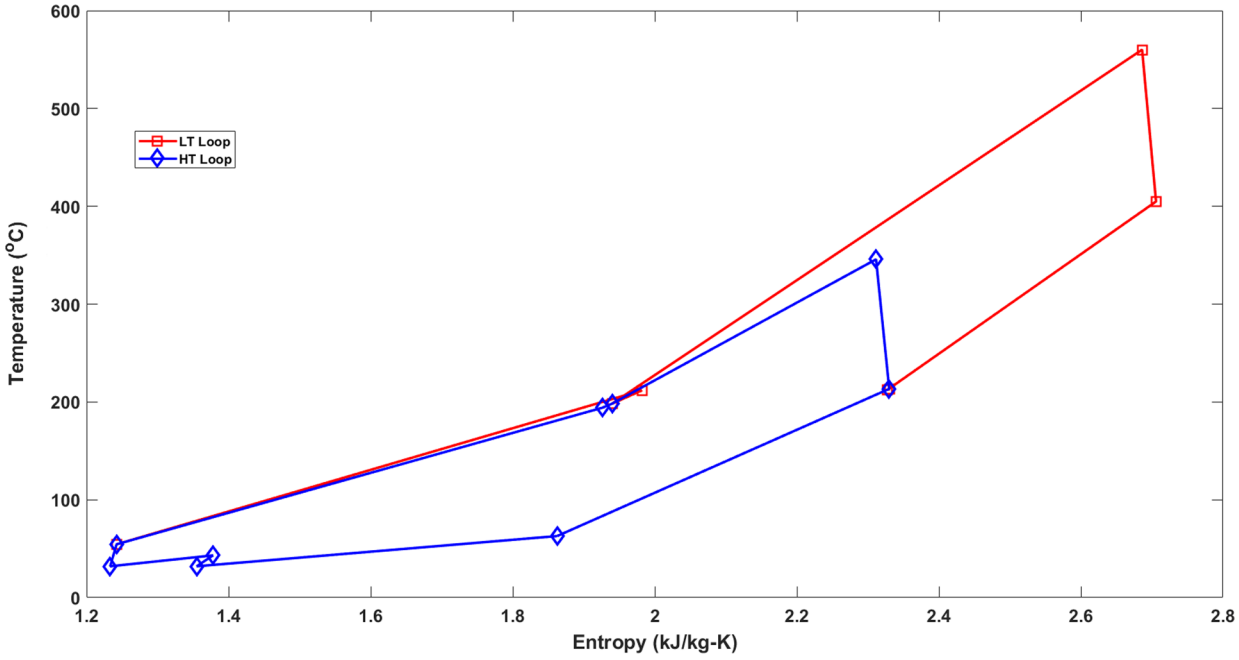

Fig. 9. Cascade Cycle 3: TS Diagram.

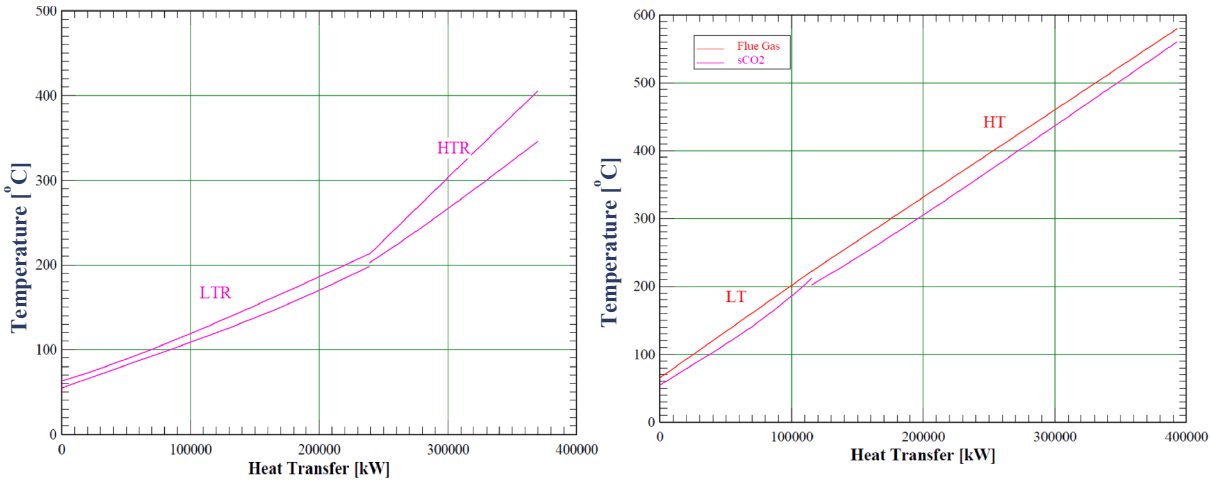

Fig. 10. T-Q Diagram of Cascade Cycle 3: Left- Recuperators, Right- Flue gas Heat exchanger.

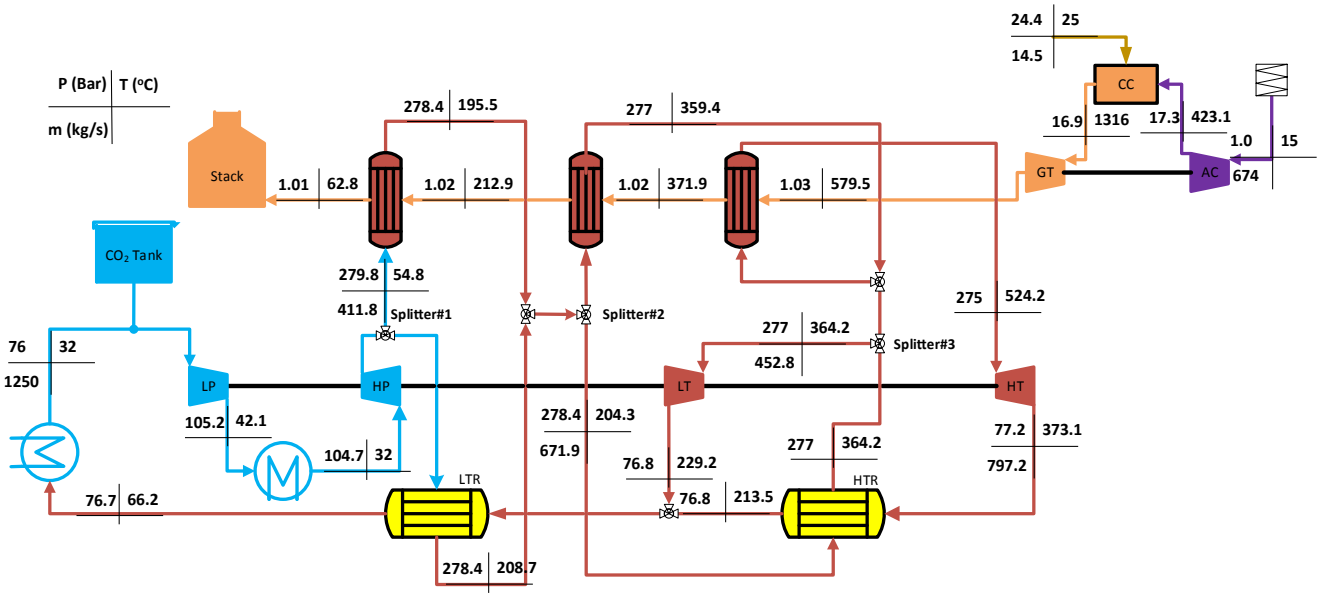

Fig. 11. Cascade Cycle 4 Configuration (Cycle 4).

$$T_o = T_i * \left(\left(\frac{P_o}{P_i} \right)^{\frac{R*\eta_p}{\bar{c}_p}} \right) \tag{7}$$

where the P_o, P_i are the pressure at the outlet and the inlet respectively, R is the gas constant, η_p is the polytropic efficiency, $\bar{c}_p$ is the average specific heat and T_o, T_i are the absolute temperature at the outlet and the inlet respectively.

The sCO_2 turbine was modelled based on isentropic efficiency using Eq. (8),

$$h_{o,turb} = h(P_o, s_i) * \eta_{i,turb} \tag{8}$$

The sCO_2 compressor was modelled based on isentropic efficiency using Eq. (9),

$$h_{o,comp} = \frac{h(P_o, s_i)}{\eta_{i,comp}} \tag{9}$$

where h is the enthalpy and s is the entropy.

The heat exchangers were modelled based on effectiveness method using Eq. (10) and the heat exchanger is discretized into sub-heat exchangers in order to capture the variation of the fluid properties along the path,

$$\epsilon = \frac{Q}{Q_{max}} \tag{10}$$

The maximum possible heat transfer is calculated as the product of flow rate and enthalpy change of the stream with lesser heat capacity if it were to be heated (or cooled) through the temperature range corresponding to the two incoming temperatures [32]. Thermoflex, on the other hand, reduces this maximum possible heat transfer if achieving that would result in a negative temperature difference anywhere in the path; essentially setting the maximum heat transfer to be the heat transfer that occurred with a pinch temperature difference of zero somewhere within the heat exchanger. Since sCO_2 properties are highly variable, the pinch point can occur within the heat-exchanger thus the heat exchanger sizing (heat transfer and the conductance) can be very different between the two methods for the same value of effectiveness. This effect can be very pronounced if the operating parameters are close to a critical point. The effectiveness values stated in this paper used the Thermoflex approach as the modelling has been done in Thermoflex.

Table 2 shows the variable ranges considered in the optimisation. However, in a few exceptional cases, the ranges have been increased, particularly the mass flow lower bound, to capture the complete Pareto front.

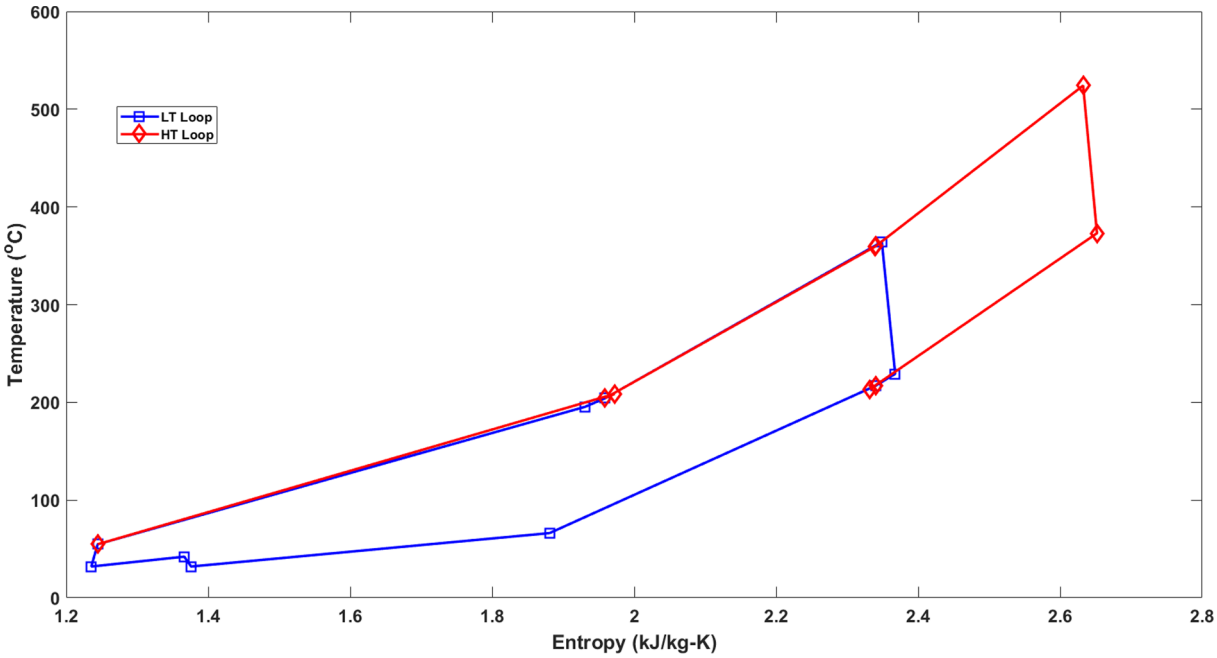

Fig. 12. Cascade Cycle 4: TS Diagram.

3.2. Optimisation Algorithm

Multi-objective optimisation is optimising (i.e. maximising or minimising) more than one objective function simultaneously subject to equality and non-equality constraints. An individual X(a) is said to be a dominant solution if X(a) is better than other solutions in all objective functions or X(a) is strictly better than other solutions in at least one objective subjected to the constraints [33]. A non-dominated Sorting Genetic Algorithm (NSGA II) was linked with the Thermoflex model via excel VBA [34] to perform the optimization study and the flowchart of the code is shown in Fig. 17 [35].

Simulation in Thermoflex tends to be slow when simulating sCO_2 cycles due to the inherent delay in calculating the thermodynamic state properties from the computationally heavy REFPROP. Despite the simulation speed and lack of compatibility to parallelize the simulation in thermoflex, the number of generation and populations were selected to be 10 times the number of variables to be optimised to ensure a globally optimal solution. The crossover and mutation probability were selected based on a few test runs. Two different objective functions were considered: (1) maximize net efficiency and specific power, (2) maximize net efficiency and minimize cost per unit electricity generation. The uncertainty of the sCO_2 component cost functions are higher, therefore, the maximum efficiency and the minimum cost designs have to be explored by the optimisation algorithm. Thus, a multi-objective optimisation is considered as opposed to single-objective cost-based optimisation.

From the Pareto front, the optimal solution is chosen to compare different cycles using a linear programming technique for multi-dimensional analysis of preference (LINMAP) decision-making [36,37]. This method chooses a solution which has a minimum Euclidean distance from the ideal solution for a set of given weights to all the objective functions assumed in the study. F_{ij} is the objective function matrix where i is the index of each point in the Pareto front and j is the index of each objective function. Then the non-dimensionalised objective function (F_{ij}^n) can be calculated by Eq. (11),

$$F_{ij}^n = w_j * \frac{F_{ij}}{\sqrt{\sum_{i=1}^{n} F_{ij}^2}} \tag{11}$$

where w_j is the weight of j^{th} objective function and $\sum_{j=1}^{m} W_j = 1$.

The Euclidean distance (d_{i+}) from the ideal solution can be calculated by Eq. (12),

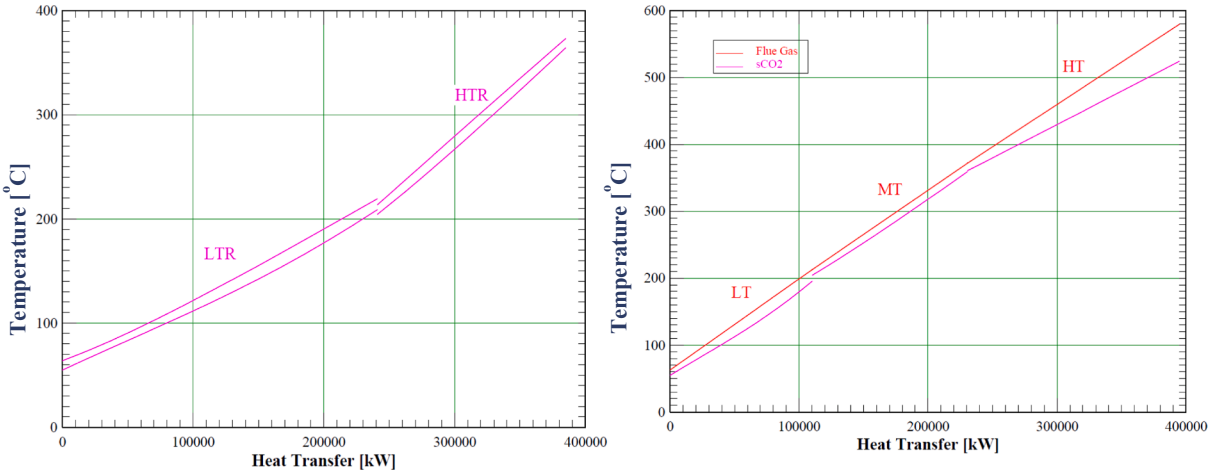

Fig. 13. T-Q Diagram of Cascade Cycle 4: Left- Recuperators, Right- Flue gas Heat exchanger.

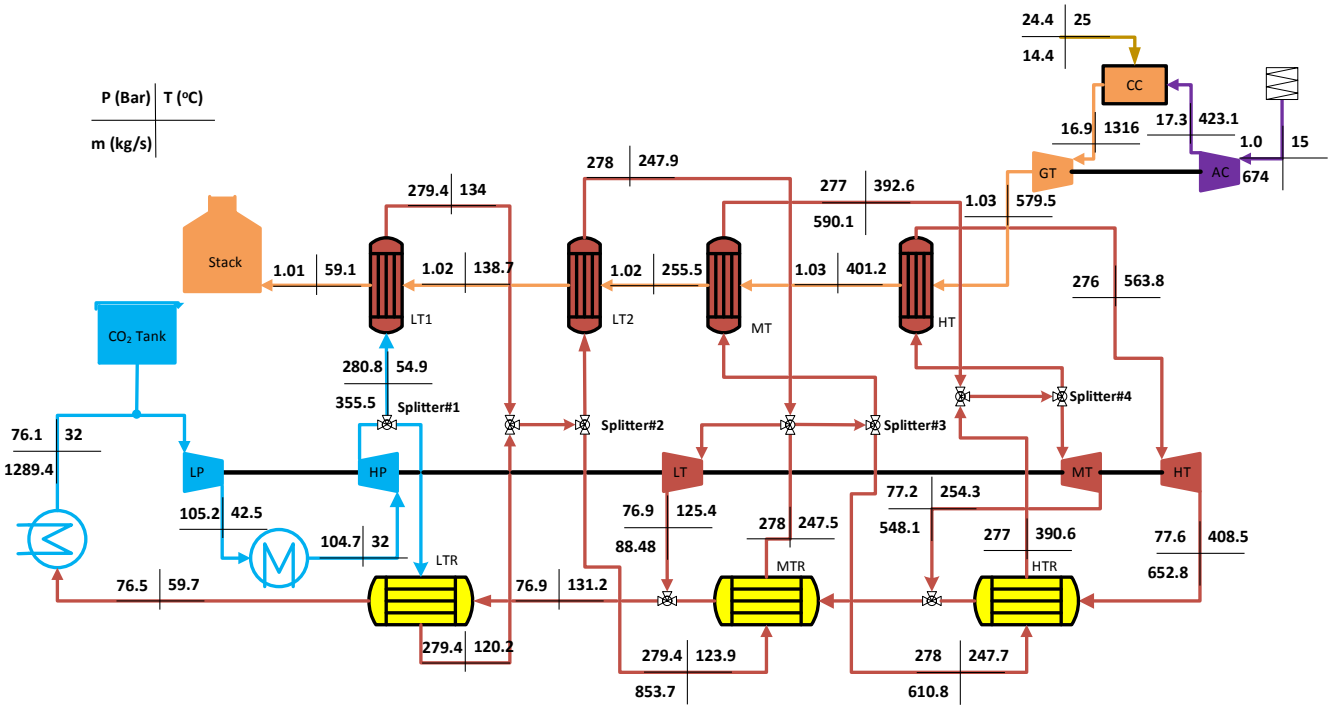

Fig. 14. Cascade Cycle 5 Configuration (Cycle 5).

$$d_{i+} = \sqrt{\sum_{j=1}^{m} (F_{ij} - F_j^{ideal})} \tag{12}$$

where F_j^{ideal} is the ideal solution of the j^{th} objective function and the ideal solution refers to the point at which each objective function is optimised in the Pareto front regardless of the other objective function. The recommended solution is having the smallest Euclidean distanced_{i+}. This study considers net efficiency and specific power/cost as objective functions.

3.3. Economic model

Various cost curves have been proposed to calculate the CAPEX of sCO_2 turbomachinery and heat exchangers. Ho et al. [38] used the cost of the heat exchanger as shown in Eq. (13) which was the fitted equation for various heat exchanger types utilising the data from ESDU [39] with a multiplication factor to account for different material. The parameters C,$/W-K and m will change for different heat exchanger fluid combination and the type.

$$Cost\,(\$) = C * (UA)^m \tag{13}$$

Marchionni et al. [40] and Wang and Dai [13] on the other hand

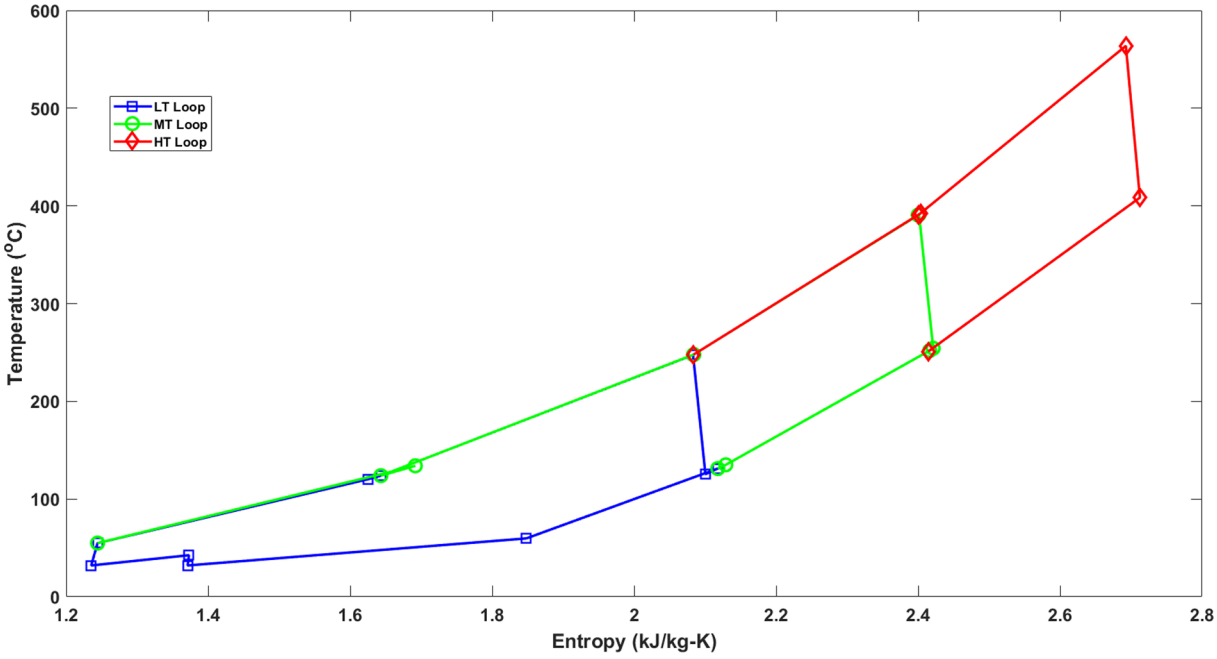

Fig. 15. Cascade Cycle 5: TS Diagram.

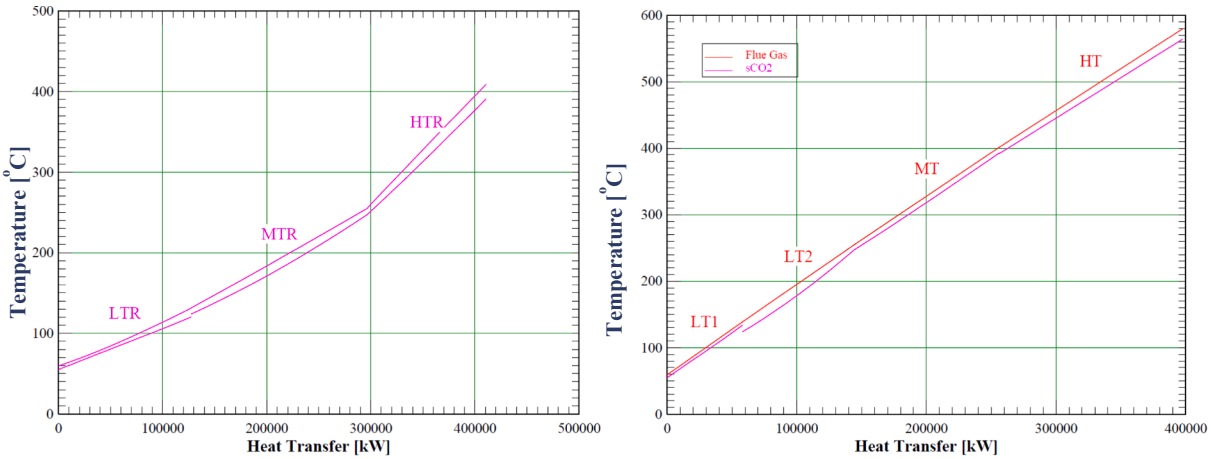

Fig. 16. T-Q Diagram of Cascade Cycle 5 Left- Recuperators, Right- Flue gas Heat exchanger.

Table 1
Thermodynamic model assumptions.

Description	Unit	Value
Air mass flow to Gas Turbine via an air compressor	kg/s	674
Polytropic efficiency of air compressor[a]	%	89.65
Polytropic efficiency of GT[a]	%	88.1
Combustor pressure loss	%	3
Fuel	–	CH_4
sCO_2 turbine isentropic efficiency[b]	%	92 [20]
sCO_2 compressor isentropic efficiency[b]	%	88 [20]
Minimum pinch	°C	3
Pressure loss in Heat exchangers	%	0.5 [20]
Effectiveness [31]	%	95 [20]
Generator Efficiency	%	98 [20]
Parasitic load[c]	MW_e	2

[a] 99.8% mechanical efficiency is considered.
[b] No mechanical losses are considered.
[c] Parasitic load accounts for the cooling system power.

proposed a function of heat exchanger area with an average value of overall heat transfer coefficient for different combinations of fluid to calculate the heat transfer area. Because the sCO_2 cycle is a highly recuperative cycle, compact heat exchangers such as Printed Circuit Heat Exchangers (PCHE) can be considered for recuperators and precooler. Zada et al. [41] proposed that the cost of PCHE is changing almost linearly as a function of conductance, the product of the overall heat transfer coefficient (U) and the heat transfer area (A), and proposed different unit rates for HTR and LTR due to the different operating temperatures which requires to have different materials.

The flue gas heat exchanger is most likely to be the same as a conventional HRSG arrangement as the limiting factor is the exhaust gas heat transfer coefficient by convection which represents 85–95% of the overall thermal resistance, hence the size should be of similar magnitude [22]. Wright et al. [21] proposed First of a Kind (FOAK) cost functions as a function of UA and this is a conservative estimate. Since the purpose of this study is not to compare the cost reduction potential against a steam Rankine cycle but rather to compare different sCO_2 cycle maximum performance and optimal GT requirements, the FOAK cost functions were considered.

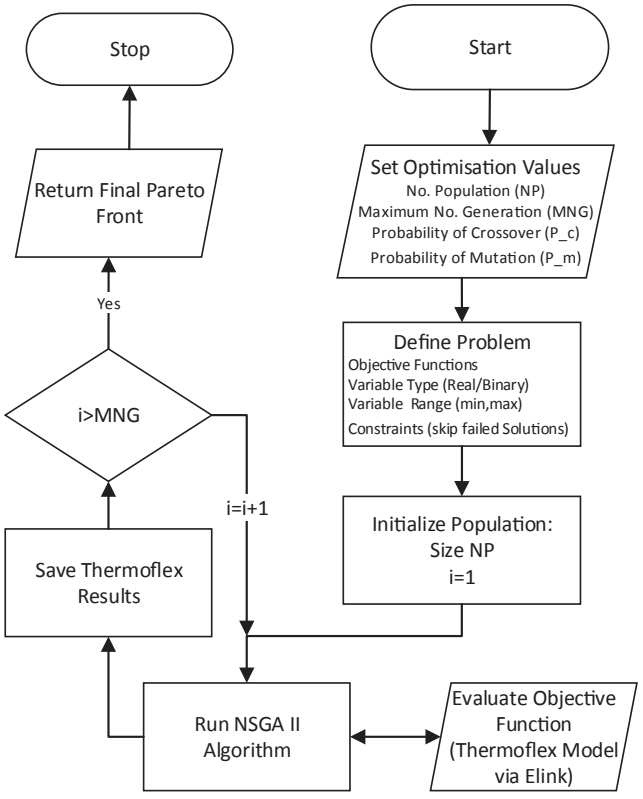

Fig. 17. NSGA II Algorithm Flowchart Used in this Study.

To calculate the cost of sCO_2 turbomachinery, this study also considers FOAK cost functions proposed by Wright et al. [21] as this also includes the conservative estimate of generator cost and other Balance

Table 2
Variable ranges of parameters considered in optimisation.

Range	Pressure ratio[a]	Max. Pressure (bar)	Min. Pressure (bar)	Intermediate Pressure[b] (bar)	SF#1*	SF#2*	SF#3*	sCO_2 Mass Flow (kg/s)
min	10	200	74	100	0.1	0.1	0.1	1000
max	35	300	90	175	0.9	0.9	0.9	1400

* SF- Split Fraction.
[a] Air compressor pressure ratio.
[b] Upstream pressure of the intercooler in sCO_2 cycle.

of Plant (BOP). Table 3 shows the list of cost functions used to calculate the CAPEX of every component in the cycle and Table 4 shows the constants used in Table 3.

The Capital Recovery Factor (CRF) is calculated by Eq. (14),

$$CRF = i * \frac{(1+i)^n}{(1+i)^n - 1} \tag{14}$$

The Cost Rate (CR, $/s) is calculated by Eq. (15),

$$CR = \frac{CRF * MF * \sum Z_i}{OH * 3600} \tag{15}$$

where Z_i is the CAPital EXpenditure (CAPEX) of i^{th} component, and MF, OH are given in Table 5.

The total cost rate is the summation of CR and Fuel Rate (FR, $/s) whilst the latter is calculated by Eq. (16),

$$FR = \frac{LHV * m_{dot} * FC}{10^6} \tag{16}$$

where m_{dot} is the fuel flow, kg/s.

The cost of unit electricity generation (c$/kWh) is calculated by Eq. (17),

$$Cost = \frac{FR * 3600 * 10^5}{NetPower} \tag{17}$$

The economic model assumptions are shown in Table 5.

4. Comparison with Literature

The thermodynamic model Pareto front is validated against the results published by Cho et al. [20] for SGT5-4000F machine as his work optimised the bottoming cycle parameters to maximise the net energy generation with errors shown in Table 6. Although Cho et al. modelled the heat exchanger based on the discretized ε-NTU method in this study the heat exchangers were sized by explicitly specifying the outlet fluid temperature owing to a different definition of effectiveness in Thermoflex. Moreover, the sCO_2 mass flow is optimised to maximise the net power generation with relaxed heat exchanger outlet temperature boundary condition. Since the error percentage is small, the thermoflex model is considered acceptable.

5. Results and discussion

5.1. Cascade Cycle 1

This cycle with intercooler achieves maximum net efficiency of 56.6% for a GT TIT of 1316 °C at the pressure ratio of 25.0. The maximum specific power of SGT5-4000F machine, operating in a simple cycle, occurs at the air compressor pressure ratio of 15.1, 16.9 and 19.7 for a GT TIT of 1216 °C, 1316 °C and 1416 °C respectively. The corresponding GT specific powers are 367.1, 424.4 and 484.9 kJ/kg respectively. Fig. 18 highlights the design which is selected based on a LINMAP algorithm giving equal weight to maximising net efficiency and minimising the cost (referred henceforth as the cost Pareto front) and maximising both GT specific power and CC efficiency (referred henceforth as the thermal Pareto front). The maximum efficiency of Cycle 1 is significantly lower than the equivalent Cycle 2 performance (i.e. 3%). This cycle has not, therefore, been analysed at different GT TIT's although this cycle can be considered in small scale WHR applications owing to its compact footprint.

5.2. Cascade Cycle 2

For a combined cycle power plant the CC specific power has to be maximised. For a steam-based CCPP, CC specific power is maximum at lower pressure ratios than the pressure ratio of maximum GT specific power. This is because the exhaust gas heat can be utilised by the HRSG. But it is not clear whether maximising the GT specific power and

Table 4
Value of constants for the cost functions listed in Table 3.

Constants in Table 3	Unit	Value
A_1 [42]	$-s/kg	266.3
A_2 [42]	$-s/kg	39.5
A_3 [42]	$-s/kg	25.6
A_4 [21]	$-K/$W_{th}$	1.7
A_5 [21]	$-K/$W_{th}$	2.5
A_6 [21]	$/kW$_e$	1000
A_7 [21]	$-K/$W_{th}$	5

Table 5
Economic model assumptions.

Description	Unit	Value
Life Time (n)	Years	20 [13]
Interest Rate (i)	%	12 [13]
Annual Operating Hours (OH)	Hrs	8000 [13]
Maintenance Factor (MF)	–	0.06 [13]
Fuel Cost (FC)	$/GJ	4 [44]
Fuel LHV (LHV)	kJ/kg	50,047 (Thermoflex)

Table 3
Component cost functions.

Components	Cost Function ($)
Gas turbine (Turbo-expander)* [42]	$\frac{C_1 * A_1 * m_{gas}\left(\frac{kg}{s}\right) * \ln(PR) * \left(1 + e^{(0.036*(T_{out}(K) - 54.4*C_2))}\right)}{0.92 - \eta_T}$
Air compressor* [42]	$\frac{C_1 * A_2 * m_{air}\left(\frac{kg}{s}\right) * PR * \ln(PR)}{0.9 - \eta_c}$
Combustor* [42]	$\frac{C_1 * A_3 * m_{air}\left(\frac{kg}{s}\right) * \left(1 + e^{(0.018*(T_{out}(K) - 26.4*C_2))}\right)}{0.995 - \frac{P_{out}}{P_{in}}}$
Precooler (water)	$A_4 * UA\,(W_{th}/K)$
Intercooler (Water)	$A_4 * UA\,(W_{th}/K)$
HT Recuperator	$A_5 * UA\,(W_{th}/K)$
LT Recuperator	$A_5 * UA\,(W_{th}/K)$
Turbomachinery + Generator + Mtotor + Gear + Piping + Skid + I&C + Aux.BOP Cost	$A_6 * Power\,(kW_e)$
Flue gas-sCO_2 Heat exchanger	$A_7 * UA\,(W_{th}/K)$

$C_1 = 1.051$ [42].
$C_2 = 1.207$ [42].
* Inflation correction is added (71%) [43].

Table 6
Comparison of model results (GT TIT = 1316 °C and Pressure Ratio = 17.2).

Cycle Layout	sCO_2 mass flow (kg/s)			Net Efficiency (%)			Bottoming Cycle Net Power (MW)		
	Literature [20]	Model	Error (%)	Literature [20]	Model	Error (%)	Literature [20]	Model	Error (%)
Cycle 1 w/o intercooling	1240	1260	1.6%	56.1	56.1	0.0%	118.5	118.5	0.0%
Cycle 1 with intercooling	1200	1195	−0.4%	56.3	56.3	0.0%	120.0	120.1	0.0%
Cycle 2 w/o inter cooling	1290	1316.7	2.1%	58.1	57.9	−0.2%	132.6	131.6	−0.7%
Cycle 2 with intercooling	1290	1286.7	−0.3%	58.5	58.5	0.1%	135.4	135.9	0.4%
Cycle 3 with intercooling	1300	1288.9	−0.9%	59.1	59.1	0.1%	139.9	140.2	0.2%

CC specific power are conflicting objectives or not at a higher pressure ratio range. Fig. 19 shows the variation of the Cycle 2 pressure ratio for three Pareto fronts (1) maximising GT specific power and CC efficiency (2) maximising CC specific power and CC efficiency (3) minimising COE and maximising CC efficiency. Examining Fig. 19, it is evident that maximising the CC specific power and GT specific power are converging to the same solution in the thermal Pareto front until the maximum GT specific power is reached. Beyond which the CC specific power continues to increase at lower GT pressure ratios whilst GT specific power reduces (not an optimal solution, therefore, discarded in the Pareto front). Minimising the COE, on the other hand, yields a different design in the cost Pareto front although the pressure ratio that corresponds to the minimum COE design is roughly equivalent to the pressure ratio at which maximum GT specific power occurs (Fig. 19). It's worth highlighting that the cost Pareto front and the thermal Pareto front are converging to the same plant design at higher CC efficiency and this confirms that the optimisation models are finding their globally optimal solutions.

Fig. 20 shows the thermal Pareto front and the corresponding air compressor pressure ratio for all the three GT inlet temperatures modelled. The maximum efficiency and GT specific power of cascade Cycle 2 with intercooler for the base case for a GT TIT of 1316 °C (equivalent to SGT5-4000F) are 58.5% and 414 kJ/kg respectively. Although the efficiency is equal to the reported Cycle 2 efficiency by Cho et al. [20] for SGT5-4000F machine, the GT pressure ratio is different (i.e. 26 in this study as opposed to 17.2 for SGT5-4000F machine). The reason is that Cho et al. [20] considered the conventional effectiveness method for sizing the heat exchanger whilst the definition of heat exchanger effectiveness is different in Thermoflex as explained in Section 3.1. In the Thermoflex method, the maximum heat transfer can be equal or lower than the conventional effectiveness method for a given effectiveness as the maximum heat transfer is reduced when the second-law is violated along the path of the heat exchanger. Additionally, this study considered a 2 MW_e parasitic load to account for the circulating water pumping power which was not considered in the work by Cho et al. [20]. Hence the calculated efficiency in this work is always lower than the reported value in Cho et al. [20] for the same GT pressure ratio.

The GT pressure ratio was increased to achieve a maximum combined cycle efficiency whilst the GT specific power reduces as shown in Fig. 20. Interestingly, the GT pressure ratio was increasing as the GT TIT increases, which indicates that the maximum combined cycle efficiency and minimum cost can be obtained within a narrow range of GT pressure ratios. Maximum efficiencies of 56.5, 58.5, and 60.2 were obtained for a GT TIT of 1216 °C, 1316 °C, and 1416 °C respectively. The corresponding GT pressure ratios are 22.6, 26.0, and 33.1. On the other hand, maximum GT specific power of 366, 423, 483 kJ/kg are obtained at the pressure ratio of 15.1, 17.5, 19.7 for a GT TIT of 1216 °C, 1316 °C, and 1416 °C respectively. From a thermal performance standpoint, the optimal pressure ratio can be defined as the pressure ratio which will give maximum CC efficiency [45].

The pressure ratio corresponds to maximum CC efficiency is not close to the pressure ratio that yields maximum GT specific power as shown in Table 7. Since the efficiency is changing very little at higher pressure ratios (Fig. 20) a small reduction in efficiency can change the pressure ratio and specific power by a significant amount. Table 7 shows the efficiency, specific power and pressure ratio of three cases (1) maximum CC efficiency (2) maximum GT specific power (3) 85% weight to CC efficiency and 15% weight to GT specific power. The weights of 85:15 for Case3 is chosen to have a 0.1% point reduction in CC efficiency to all the different GT TIT cases. The specific power range between maximum specific power and maximum efficiency has reduced

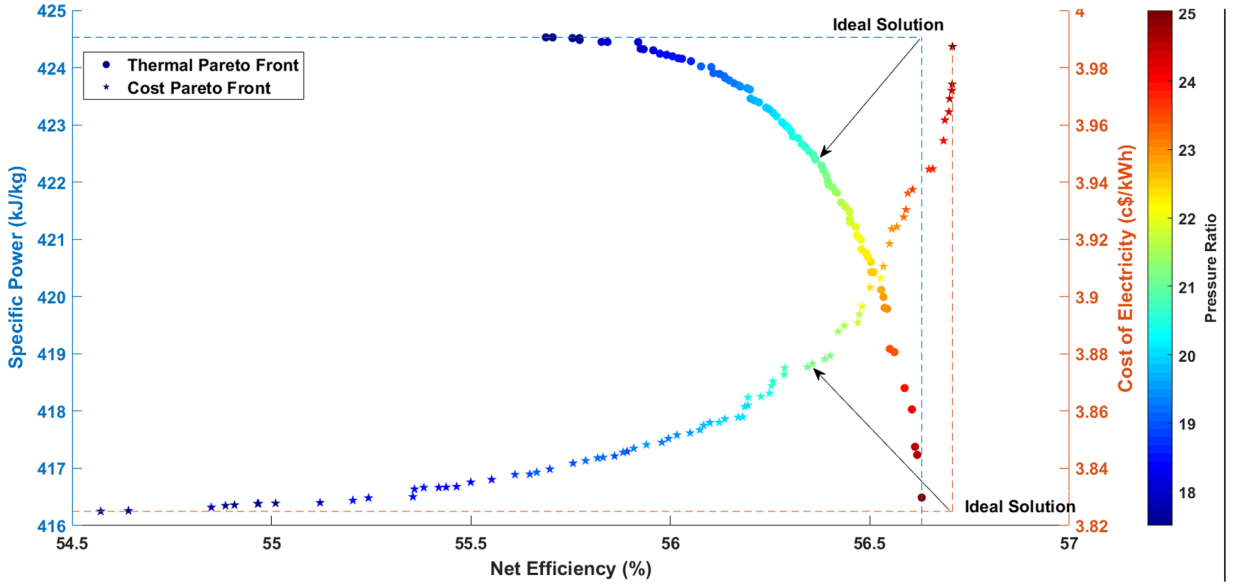

Fig. 18. Cycle 1 Cost Pareto Front at GT TIT-1316 °C.

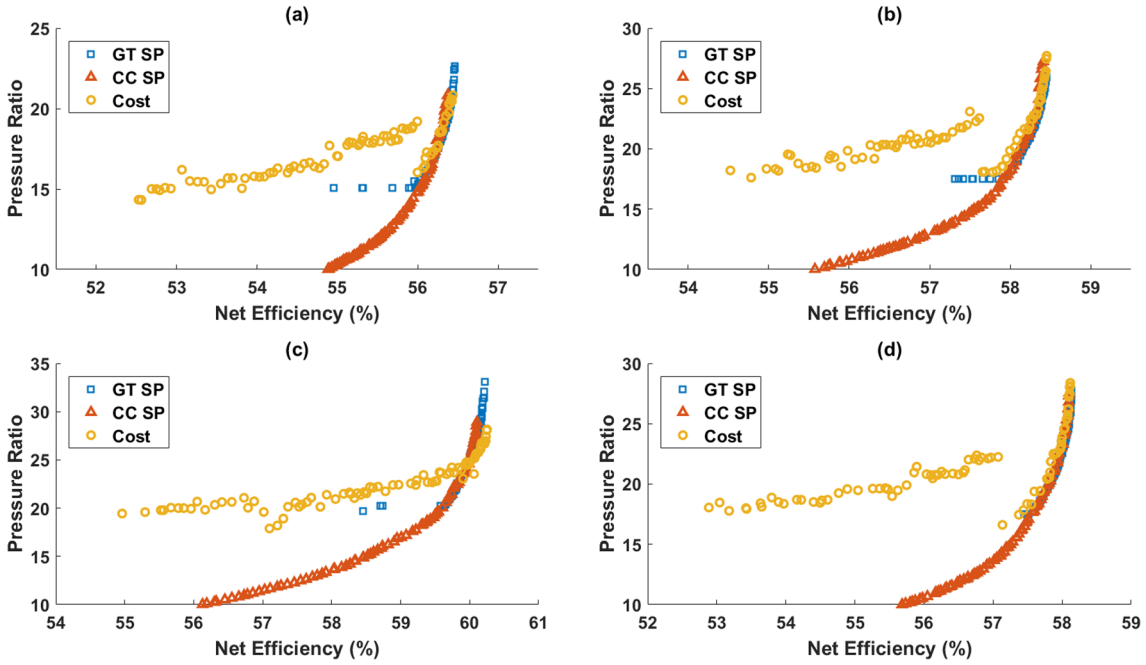

Fig. 19. Pressure ratio of Cycle 2 for three Pareto fronts: (a) GT TIT-1216 °C, (b) GT TIT-1316 °C, (c) GT TIT-1416 °C, (d) GT TIT-1316 °C w/o intercooler.

by 62% and the pressure ratio at maximum efficiency case was reduced by ~15% for a GT TIT 1216 °C. The reduction in pressure ratio of 85:15 case from the pressure ratio of maximum GT specific power case is 4.3, 5.4 and 7.3 for a GT TIT of 1216 °C, 1316 °C, and 1416 °C respectively. It is clear that at lower GT TIT the pressure ratio of maximum GT specific power case and 85:15 ratio case is proximate and it diverges as the GT TIT increases. This implies that Cycle 2 can better integrate with lower GT TIT's for which the optimal pressure ratio can be chosen with a smaller trade-off in specific power and CC efficiency. It is worth highlighting that since the pressure ratio at maximum CC efficiency (i.e. optimal pressure ratio) is 26.0 for a GT TIT of 1316 °C which is higher than the equivalent SGT5-4000 machine pressure ratio (i.e. 17.2), then integration of an sCO_2 cycle with a commercially operating GTs cannot achieve the maximum performance as a fully flexible CCPP design with a sCO_2 bottoming cycle. This is because the pressure ratio of conventional CCPP for maximum efficiency is close to maximum GT specific power [45], therefore, the commercial GT's pressure ratio is proximate to maximum GT specific power. Although the pressure difference between Case2 and Case3 are relatively smaller at GT TIT of 1216 °C, the difference diverges as the GT TIT increases. This questions the ability to integrate Cycle 2 with higher TIT GTs. Therefore, the sCO_2 cycle configuration plays a critical role in integrating a sCO_2 bottoming cycle with a commercially available GT. The energy share from the bottoming cycle (ratio between the net power from sCO_2 cycle and CC net

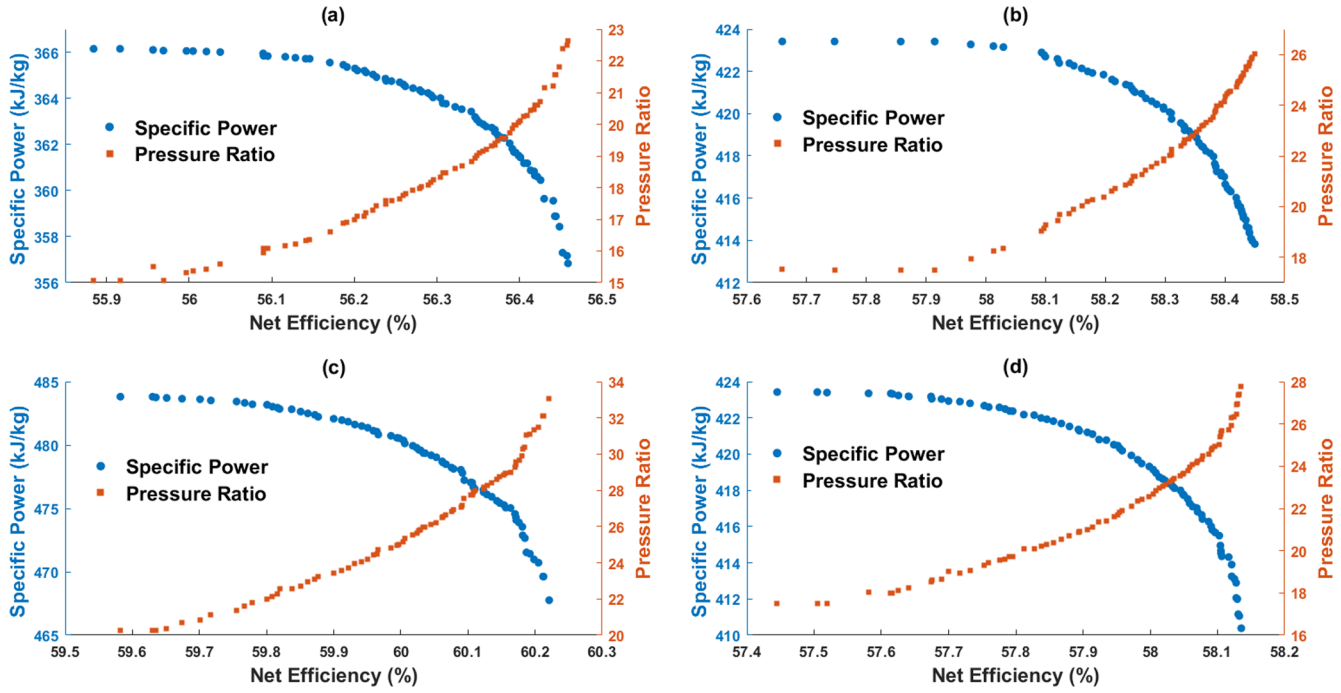

Fig. 20. Cycle 2 Thermal Pareto fronts: (a) GT TIT-1216 °C, (b) GT TIT-1316 °C, (c) GT TIT-1416 °C, (d) GT TIT-1316 °C w/o intercooler.

Table 7
Cycle 2: Three cases from thermal Pareto front for a GT TIT of 1216 °C, 1316 °C and 1416 °C.

GT TIT (°C)	Efficiency (%)			Specific Power (kJ/kg)			Pressure Ratio			% Share Bot.cycle [d]		
	Case1[a]	Case2[b]	Case3[c]	Case1[a]	Case2[b]	Case3[c]	Case1[a]	Case2[b]	Case3[c]	Case1[a]	Case2[b]	Case3[c]
1216	56.5	55.0	56.4	356.8	366.2	362.6	22.6	15.1	19.3	28.1	31.6	29.9
1316	58.5	57.3	58.4	413.8	423.4	418.9	26.0	17.5	22.9	27.7	31.4	29.0
1416	60.2	58.5	60.1	467.8	483.9	478.0	33.1	19.7	27.0	26.3	30.4	28.3
1316[e]	58.1	57.4	58.0	410.4	423.4	418.0	27.8	17.5	23.5	26.7	31.5	28.5

[a] Maximum efficiency case.
[b] Maximum GT specific power case.
[c] 85:15 wt between efficiency and specific power respectively in LINMAP.
[d] Power output share from the bottoming cycle.
[e] Without intercooler case.

power) reduces as the GT TIT increases at maximum efficiency point (see Table 7- Case 1). This is because, although the GT pressure ratio increases with the GT TIT, the consequential increase in TET is lower, which reduces the bottoming cycle energy share. This indicates that the energy losses from the bottoming cycle at higher GT TITs are relatively higher than the losses from the topping cycle, therefore, the topping cycle energy share increases with the GT TIT in order to maximise whole plant efficiency. This is also true for a steam-based bottoming cycle [24]. Moreover, it is worth highlighting that the bottoming cycle energy share is higher for the case with intercooler than without intercooler because the intercooler reduces the sCO_2 temperature to the low-temperature exhaust heat exchanger, aiding heat recovery, thereby making the bottoming cycle more efficient. The bottoming cycle energy share for a triple-pressure steam Rankine cycle with the commercial SGT5-4000F is around ~32.1%, which is higher than this sCO_2 cycle.

The maximum efficiency from the cost Pareto front is 58.5% and this is attained at a GT pressure ratio of 29.1 for a GT TIT of 1316 °C. The maximum efficiency obtained from cost Pareto front is the same as the thermal Pareto front, nevertheless, the pressure ratio is different. This is because the efficiency change plateaus at a higher pressure ratio. Despite a few scatter points of pressure ratio in the cost Pareto front, in general, the pressure ratio was found to increase with the increase in the net-efficiency as shown in Fig. 21. There is a discontinuity in the change in pressure ratio for GT TIT 1316 °C and 1416 °C which was caused by the step change of the split ratio to the low-temperature recuperator (not plotted here). Table 8 shows three cases of the cost Pareto front (1) maximum CC efficiency (2) minimum COE (3) 95% weight to CC efficiency and 5% weight to COE. The weight of 95:5 is considered in the cost domain in order to maintain the efficiency difference by 0.1% point from the maximum efficiency. The pressure ratio difference between Case2 and Case3 are increasing as the GT TIT increases from 1216 °C to 1416 °C. This infers that the trade-off range of pressure ratios is higher for higher GT TIT and this emphasises that Cycle 2 cannot integrate well for higher GT TIT cases to realise the maximum economic benefit. The minimum cost pressure ratio is apparently close to the pressure ratio that yields maximum GT specific power (Table 8- case2). The energy share from the bottoming cycle is reduces as the GT TIT increases. The bottoming cycle energy share reduces for both minimum cost case and maximum efficiency case (Table 8- case1 and 2) and that is roughly close to each other.

The intercooler in Cycle 2 increases the maximum net efficiency by ~0.4% point with the increased COE of ~1%. The intercooler increases

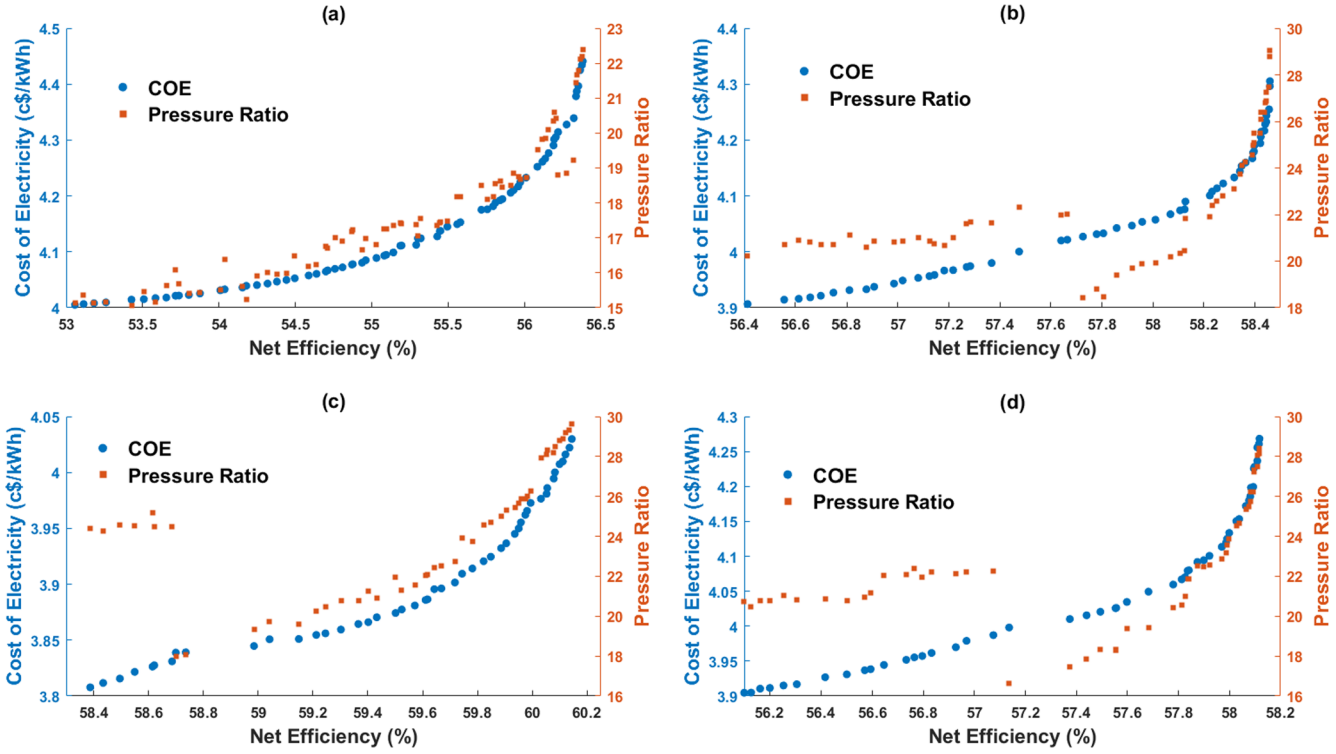

Fig. 21. Cycle 2 Cost Pareto fronts: (a) GT TIT-1216 °C, (b) GT TIT-1316 °C, (c) GT TIT-1416 °C, (d) GT TIT-1316 °C w/o intercooler.

Table 8
Cycle 2: Three cases from cost Pareto front for a GT TIT of 1216 °C, 1316 °C and 1416 °C.

GT TIT (°C)	Efficiency (%)			COE (c$/kWh)			Pressure Ratio			% Share Bot.cycle [d]		
	Case1[a]	Case2[b]	Case3[c]	Case1[a]	Case2[b]	Case3[c]	Case1[a]	Case2[b]	Case3[c]	Case1[a]	Case2[b]	Case3[c]
1216	56.4	52.6	56.3	4.4	4.0	4.3	22.4	14.7	19.2	29.0	29.2	29.7
1316	58.5	54.3	58.4	4.3	3.8	4.2	29.1	17.3	24.5	27.1	27.3	28.5
1416	60.3	55.0	60.2	4.1	3.7	4.0	33.2	20.2	29.6	26.3	25.6	27.4
1316[e]	58.1	52.9	58.0	4.3	3.8	4.1	28.4	18.1	23.2	26.4	25.2	28.5

[a] Maximum efficiency case.
[b] Minimum cost case.
[c] 95: 5 wt between efficiency and cost respectively in LINMAP.
[d] Power output share from the bottoming cycle.
[e] Without intercooler case.

the plant net efficiency due to (1) the reduction of compressive power (isothermal compression) and (2) lower compressor outlet temperature that aids more heat transfer from the flue gas. Cycle 2 with intercooler produces 0.8% higher specific power at the maximum efficiency condition as compared to Cycle 2 without an intercooler. The pressure ratio of the thermal Pareto front at maximum efficiency for Cycle 2 without intercooler is higher than Cycle 2 with intercooler by 1.8. The exclusion of the intercooler does not significantly change the optimal pressure ratio. The improvement in efficiency will reduce if the exhaust stack minimum temperature limitation is imposed.

The net efficiency, thermal Pareto front pressure ratio, specific power and the cost of electricity are varying almost linearly as a function of turbine inlet temperature within the range studied i.e. 1216–1416 °C. Even though there is an influence of higher-order terms, it is hard to capture with only three data points, however, a linear trend provides a reasonable fit to these data.

Fig. 22 shows the CC specific power, GT specific power, CC efficiency, and GT pressure ratio for a GT TIT of 1216 °C, 1316 °C and 1416 °C. This curve can be used approximately to estimate the expected CC efficiency and specific power for different GT TIT and pressure ratios. The CC specific powers in Fig. 22 are normalised with 577.2, 660.7 and 746.9 kJ/kg for a GT TIT of 1216 °C, 1316 °C and 1416 °C respectively and the GT specific powers are normalised to 366.2, 423.4 and 483.9 kJ/kg respectively. These curves are strictly valid for the assumed topping cycle and bottoming cycle component performance. Any deviation of the component performance can introduce some degree of uncertainty and these effects can be approximated by correcting the impact of the particular design parameter change on the efficiency (or specific power) by assuming all the variables are independently affecting the efficiency. The sensitivity of changes in CC efficiency and GT specific power for the changes in the air compressor and GT polytropic efficiency is tabulated in the sensitivity analysis section (Tables 16 and 17). It has to be noted that the estimation can only approximate the expected performance as it is neglecting the secondary effects due to the variable interdependency.

5.3. Cascade Cycle 3

Fig. 23 shows the thermal Pareto fronts for all the GT inlet temperatures studied. The maximum efficiency and specific power of cascade Cycle 3 with intercooler for the base case for a GT TIT of 1316 °C (equivalent to SGT5-4000F) are 59.1% and 415 kJ/kg, which is attained at the GT pressure ratio of 25.6. Examining Table 9, it can be seen that Cycle 3 is able to achieve higher efficiency at a relatively lower pressure ratio compared to Cycle 2. Similar to Cycle 2, the pressure ratio at maximum efficiency is proximate to the pressure ratio for maximum GT

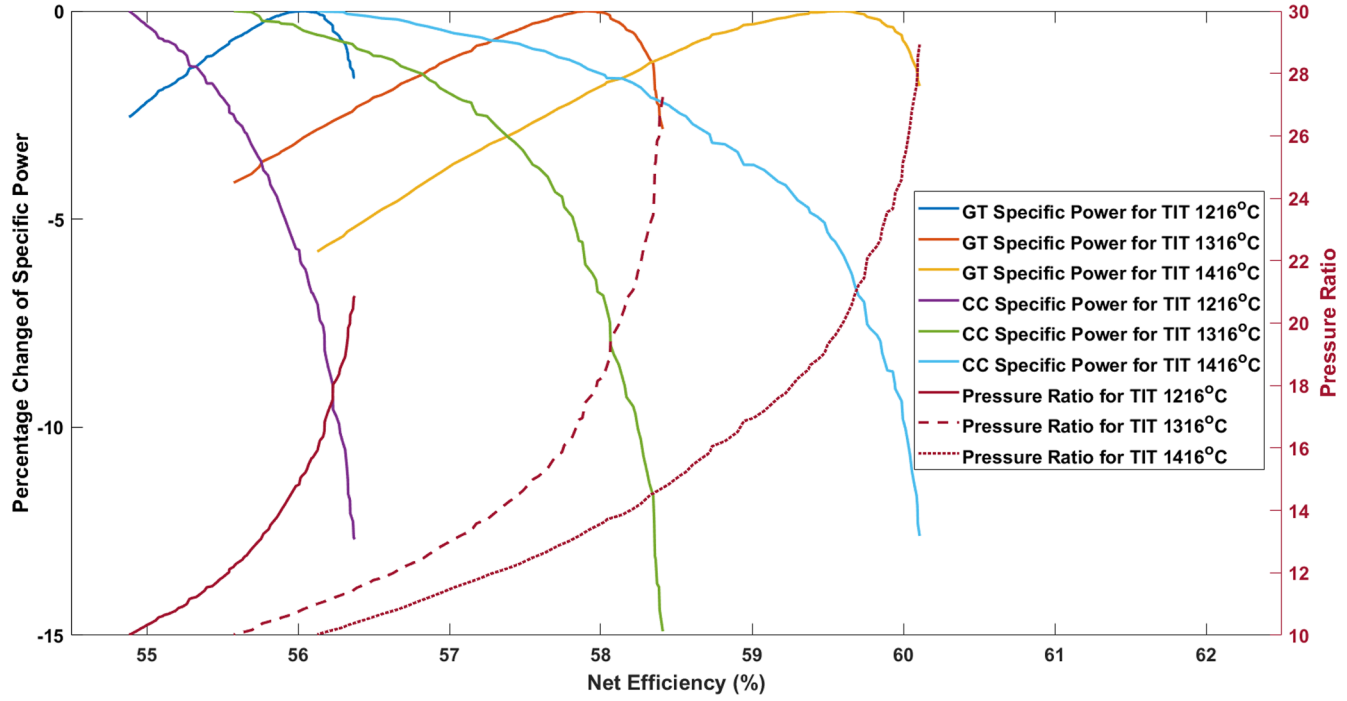

Fig. 22. Relationship between Pressure ratio, efficiency and Specific power for Cycle 2 for a GT TIT of 1216 °C, 1316 °C and 1416 °C.

specific power. The pressure ratio difference between Case2 and Case3 is roughly equal (i.e. ~6) for a GT TIT of 1316 °C and 1416 °C. Moreover, these pressure ratio differences for all the GT TIT's are lower than Cycle 2. This infers that Cycle 3 can be a good candidate compared to Cycle 2 for all the GT TIT's studied. The specific power at maximum efficiency case is higher than Cycle 2 for all the GT TIT cases. The specific power at maximum efficiency case has increased by 2.2 kJ/kg when adding an intercooler with Cycle 3 for a GT TIT of 1316 °C. Examining Table 9, the Case2 and Case3 pressure ratios with and without intercooler are roughly the same, but it is higher by 1.2 for Case1. The energy share from the bottoming cycle is higher than Cycle 2 for all the GT TITs and the share is the same for GT TIT 1316 °C and 1416 °C at maximum efficiency point. This indicates that the TET increases at higher GT TIT in order to keep the bottoming cycle energy share the same.

The cost Pareto fronts of Cycle 3 are shown in Fig. 24. The pressure ratio is not smooth as it is in the thermal Pareto front. In general, it increases as the efficiency increases for all GT TITs. Examining Table 10, the difference in pressure ratio between Case2 and Case3 are 4.7, 5.9 and 7.1 for a GT TIT of 1216 °C, 1316 °C and 1416 °C respectively. These are lower than Cycle 2 for a GT TIT of 1316 °C and 1416 °C and it is the same for a GT TIT of 1216 °C. Therefore, Cycle 3 can better integrate with GTs than Cycle 2 for higher GT TITs. The pressure ratio difference between Case2 and Case3 are a bit higher for Cycle 3 without intercooler than Cycle 3 with intercooler. In general, the pressure ratios that has the minimum cost is roughly the same as the pressure ratio of maximum GT specific power. The COE is not significantly different than Cycle 2 for Case1 and Case2.

The intercooler in Cycle 3 increases the efficiency in Case1 by ~0.4% point with the same COE without an intercooler. The pressure ratio of Cycle 3 without intercooler is higher than Cycle 3 with intercooler by 1.3. Since the efficiency improvement will be sacrificed when the stack minimum temperature limitation is imposed, the COE can go higher for Cycle 3 with an intercooler.

The efficiency and the GT specific power of a CCPP when integrating Cycle 3 for different GT TITs can be interpreted from Fig. 25. Linear interpolation across different GT TITs can be used for the temperature range studied. The CC specific powers in Fig. 25 are normalised with 585.1, 672.0 and 763.7 kJ/kg for a GT TIT of 1216 °C, 1316 °C and 1416 °C respectively and the GT specific powers are normalised to 366.2, 423.4 and 483.8 kJ/kg respectively. For an SGT5-4000F machine (Pressure ratio −17.2, GT TIT-1316 °C), integrating Cycle 3 as the bottoming cycle can offer the maximum efficiency of 58.6% whilst the maximum efficiency of 59.1% can be achieved at the pressure ratio of 23.1 (Table 9-Case3).

Maximising the GT specific power of Cycle 3 also increases CC specific power whilst maximising the CC efficiency. It is worth highlighting that this behaviour is the same as Cycle 2 and a similar trend is observed for Cycle 4, therefore, those plots not repeated for these other cycles (see Fig. 26).

5.4. Cascade Cycle 4

The maximum net efficiency of Cycle 4 thermal Pareto front is 59.5% while it is 58% for a maximum GT specific power case at GT TIT of 1316 °C as shown in Table 11 and in Fig. 27. The corresponding pressure ratio for maximum efficiency design is 24.6 whilst it is 17.5 for maximum GT specific power condition. The maximum specific power has reduced by ~1.1 kJ/kg for all the GT TITs compared with Cycle 3 and Cycle 4. This is because of the increased GT exhaust back pressure owing to the additional heat exchangers added in the flue gas path which leads to a 0.5% pressure loss. Whilst the specific power at maximum efficiency case is also lower than Cycle 3 for GT TIT 1216 °C and 1416 °C, it is a bit higher for 1316 °C with intercooler (i.e. 0.8 kJ/kg). Adding an intercooler can increase the maximum efficiency by 0.4% point with an increase of about 4.8 kJ/kg.

Examining Table 11, Cycle 4 is able to achieve higher efficiency at a relatively lower pressure ratio compared to Cycle 2 and roughly at equal pressure ratios compared to Cycle 3 (Case3). The pressure ratio difference between Case2 and Case3 is lower than the corresponding difference in Cycle 3 for a GT TIT of 1316 °C and 1416 °C. This infers that Cycle 4 can be a good candidate for higher temperatures (i.e. > GT TIT of 1316 °C). The bottoming cycle energy share is higher for a GT TIT of 1216 °C and reduces as the TIT increases. For GT TIT of 1316 °C, the energy share is 29.8% which is still lower than the steam cycle integrated with SGT5-4000F (i.e. 32.1%).

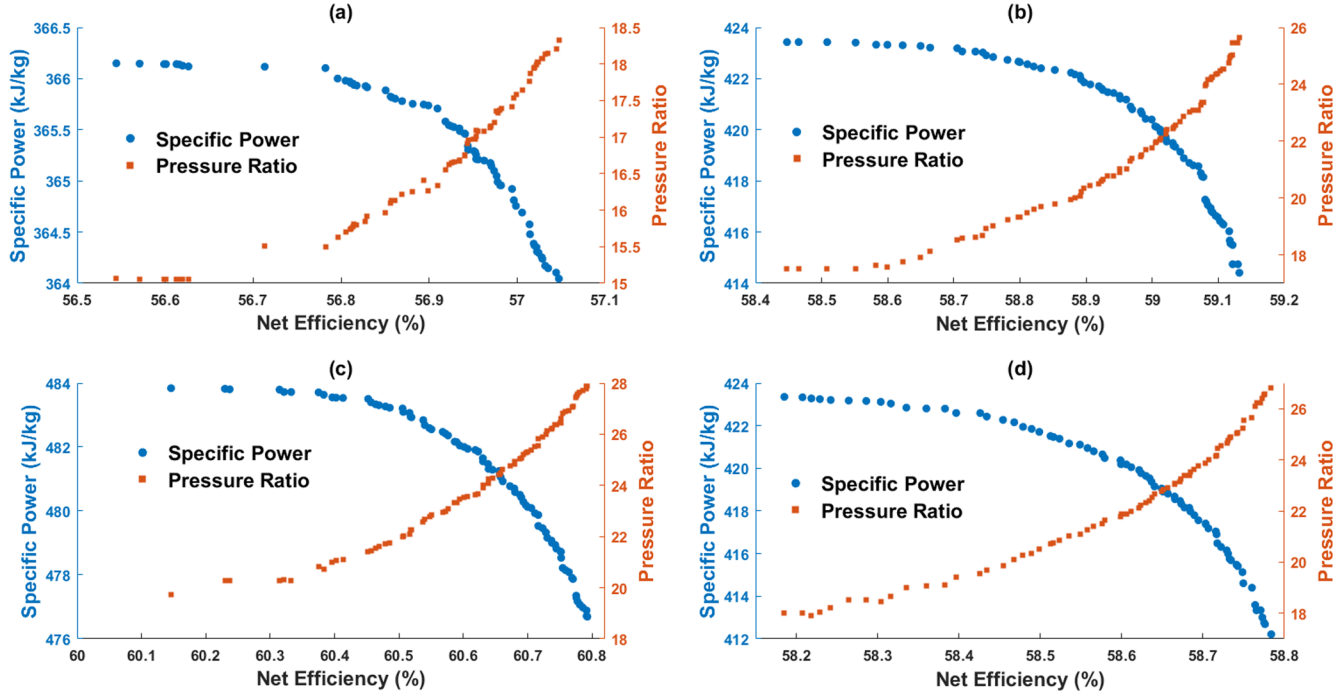

Fig. 23. Cycle 3 Thermal Pareto fronts: (a) GT TIT-1216 °C, (b) GT TIT-1316 °C, (c) GT TIT-1416 °C, (d) GT TIT-1316 °C w/o intercooler.

Table 9
Cycle 3: Three cases from thermal Pareto front for a GT TIT of 1216 °C, 1316 °C and 1416 °C.

GT TIT (°C)	Efficiency (%)			Specific Power (kJ/kg)			Pressure Ratio			% Share Bot.cycle [d]		
	Case1[a]	Case2[b]	Case3[c]	Case1[a]	Case2[b]	Case3[c]	Case1[a]	Case2[b]	Case3[c]	Case1[a]	Case2[b]	Case3[c]
1216	57.0	55.5	57.0	364.0	366.2	364.6	18.3	15.1	17.8	31.0	31.8	31.4
1316	59.1	57.0	59.1	414.4	423.4	418.6	25.6	17.5	23.1	28.4	30.7	29.5
1416	60.8	60.1	60.7	476.7	483.8	479.9	27.9	19.7	25.6	28.4	32.0	29.3
1316[e]	58.8	57.4	58.7	412.2	423.4	418.1	26.8	17.5	23.4	27.8	31.5	29.2

[a] Maximum efficiency case.
[b] Maximum GT specific power case.
[c] 85:15 wt between efficiency and specific power respectively in LINMAP.
[d] Power output share from the bottoming cycle.
[e] Without intercooler case.

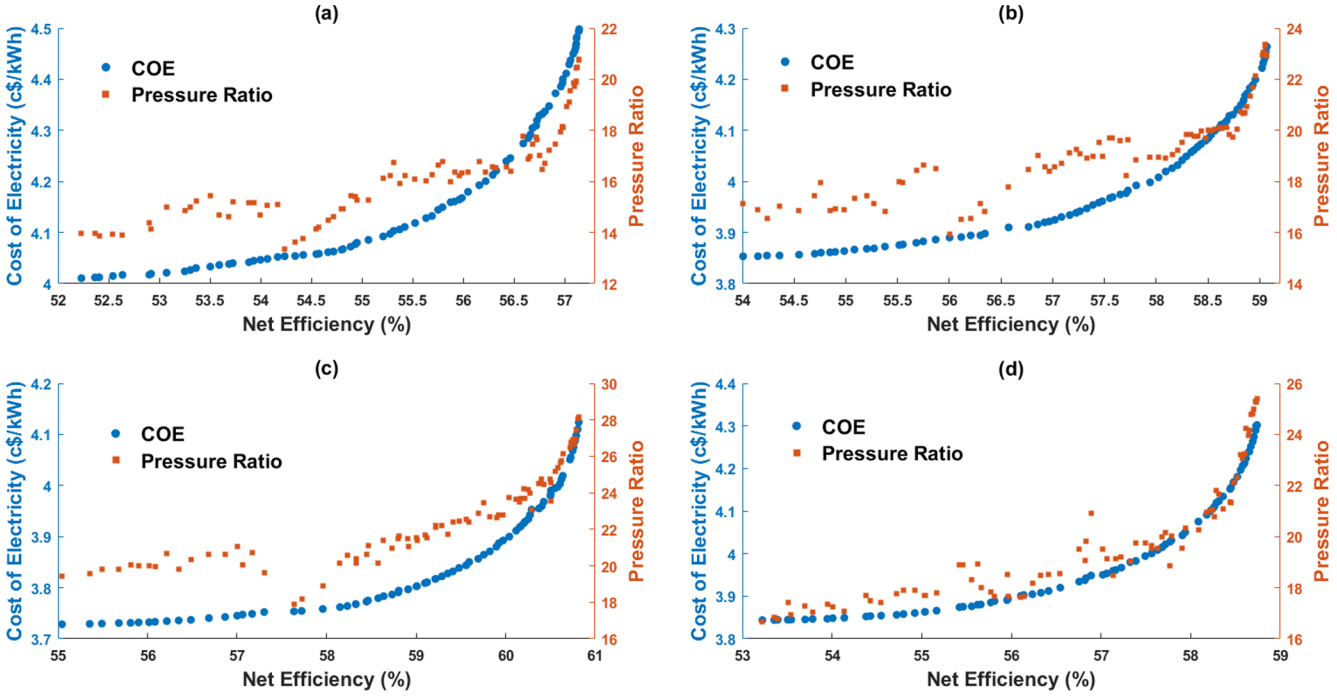

Fig. 24. Cycle 3 Cost Pareto fronts: (a) GT TIT-1216 °C, (b) GT TIT-1316 °C, (c) GT TIT-1416 °C, (d) GT TIT-1316 °C w/o intercooler.

Table 10
Cycle 3: Three cases from cost Pareto front for a GT TIT of 1216 °C, 1316 °C and 1416 °C.

GT TIT (°C)	Efficiency (%)			COE (c$/kWh)			Pressure Ratio			% Share Bot.cycle [d]		
	Case1[a]	Case2[b]	Case3[c]	Case1[a]	Case2[b]	Case3[c]	Case1[a]	Case2[b]	Case3[c]	Case1[a]	Case2[b]	Case3[c]
1216	57.1	51.9	57.0	4.5	4.0	4.4	20.8	14.2	18.9	30.1	28.8	31.1
1316	59.1	53.9	59.0	4.3	3.9	4.2	22.9	17.0	22.9	30.1	27.6	30.0
1416	60.8	55.0	60.7	4.1	3.7	4.1	28.2	19.4	26.5	28.8	26.4	29.4
1316[e]	58.7	53.2	58.7	4.3	3.8	4.2	25.4	16.7	24.2	28.4	26.9	28.8

[a] Maximum efficiency case.
[b] Minimum cost case.
[c] 95: 5 wt between efficiency and cost respectively in LINMAP.
[d] Power output share from the bottoming cycle.
[e] Without intercooler case.

Examining Case3 in Table 11, the pressure ratio, efficiency and the GT specific power are almost changing linearly as a function of GT TIT. A simulation for a GT TIT of 1366 °C has been carried out to estimate the uncertainty of linear interpolation. The linear curve fit for Case 3 predicts a CC efficiency of 60.2% for a GT TIT of 1366 °C and linear interpolation of the pressure ratio yields 24.0. The CC efficiency from the simulation for Case 3 is 60.2% that corresponds to the pressure ratio of 25.2. This confirms that linear interpolation can reasonably predict the efficiency and the optimal pressure ratio within the GT firing temperature range studied. A linear extrapolation of the optimal pressure ratio and the CC efficiency for a GT TIT of 1516 °C are 29.7 and 63% respectively. The simulation results for a GT TIT of 1516 °C yields 62.6% efficiency that corresponds to the pressure ratio of 29.1. The uncertainty of linear extrapolation for the efficiency is higher than the simulation result and it overpredicts the efficiency (i.e. the efficiency slope reduces as the GT TIT increases). The uncertainty of extrapolating

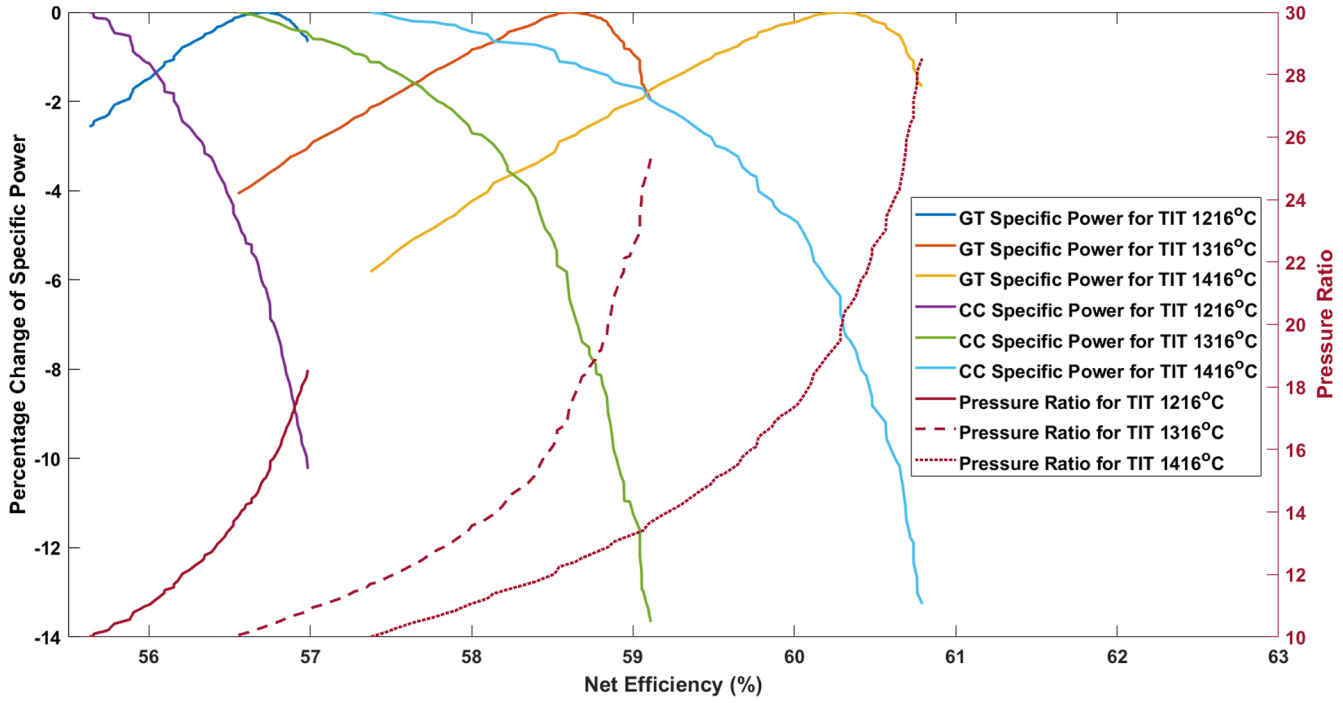

Fig. 25. Relationship between Pressure ratio, efficiency and Specific power for Cycle 3 for a GT TIT of 1216 °C, 1316 °C and 1416 °C.

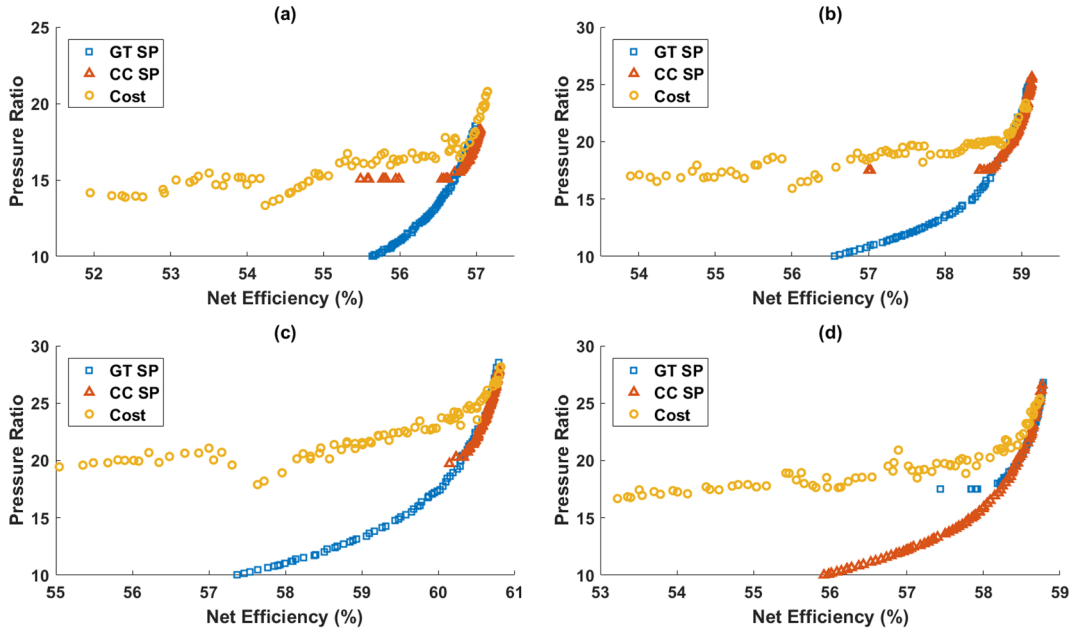

Fig. 26. Pressure ratio of Cycle 3 for three Pareto fronts: (a) GT TIT-1216 °C, (b) GT TIT-1316 °C, (c) GT TIT-1416 °C, (d) GT TIT-1316 °C w/o intercooler.

the optimal efficiency, on the other hand, is not significant for this case. The commercially available H-class machine GT TIT is approximately equal to 1516 °C, therefore, integrating Cycle 4 with the H-class size machine can reach around 63% net efficiency when optimising the pressure ratio. However, this has to be corrected for the changes in the compressor and GT polytropic efficiency compared to the values considered in this study. In order to estimate the uncertainty of extrapolation, Cycle 4 has been simulated for the GT TIT of 1516 °C and the maximum CC efficiency is 62.7% which is obtained at the pressure ratio of 31.3. Since the component efficiencies of a GT are dictated by techno-economic optimisation, the efficiency of 63% can be realisable if those component efficiencies are economically attractive. Since the pressure ratio is higher than the equivalent steam bottoming cycle, the Turbine Exhaust Temperature (TET) will be lower (~600 °C as opposed to ~650 °C), therefore, the bottoming cycle can accept better material. Nevertheless, it has to be also noted that the sCO_2 pressure (~300 bar) is higher than the equivalent steam pressure in a steam-based Rankine cycle (~175 bar) which might increase the cost.

The cost Pareto fronts are plotted in Fig. 28 for three different GT TIT's together with the pressure ratio. The pressure ratio trend is not smooth along the cost Pareto front. Examining the COE of Cycle 4 in Table 12 and comparing with Table 10 shows that the COE of Cycle 4 is higher compared to Cycle 3. This is because the efficiency improvement is not high enough to offset the increase in CAPEX which largely resulted in the reduced LMTD in the sCO_2 cycle heat exchangers. Interestingly, the pressure ratio at which maximum efficiency occurs is

Table 11
Cycle 4: Three cases from thermal Pareto front for a GT TIT of 1216 °C, 1316 °C and 1416 °C.

GT TIT (°C)	Efficiency (%)			Specific Power (kJ/kg)			Pressure Ratio			% Share Bot.cycle [d]		
	Case1[a]	Case2[b]	Case3[c]	Case1[a]	Case2[b]	Case3[c]	Case1[a]	Case2[b]	Case3[c]	Case1[a]	Case2[b]	Case3[c]
1216	57.4	57.1	57.4	362.1	365.1	363.0	19.0	15.1	18.3	31.5	34.3	32.0
1316	59.5	58.0	59.4	415.2	422.3	418.6	24.6	17.5	22.3	29.8	32.3	30.8
1416	61.1	60.8	61.1	470.1	482.6	478.4	31.3	20.3	25.8	28.1	32.8	30.1
1316[e]	59.1	58.6	59.0	410.4	422.3	417.9	25.4	18.0	22.9	28.9	32.6	30.0

[a] Maximum efficiency case.
[b] Maximum GT specific power case.
[c] 85:15 wt between efficiency and specific power respectively in LINMAP.
[d] Power output share from the bottoming cycle.
[e] Without intercooler case.

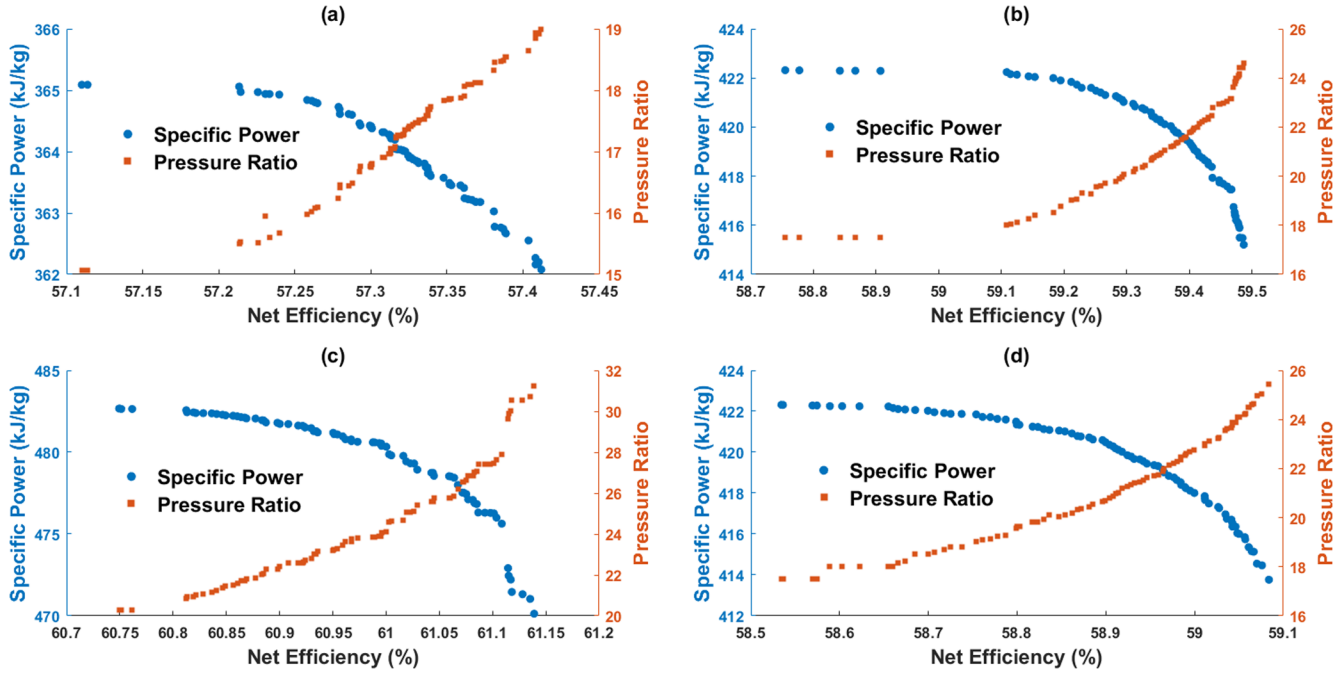

Fig. 27. Cycle 4 Thermal Pareto fronts: (a) GT TIT-1216 °C, (b) GT TIT-1316 °C, (c) GT TIT-1416 °C, (d) GT TIT-1316 °C w/o intercooler.

lower than Cycle 2 and this implies that Cycle 4 can better integrate with a GT with higher TET owing to its increased flexibility.

Although the pressure ratio at maximum efficiency of Cycle 4 is a bit lower than Cycle 3, for a GT TIT of 1416 °C, it is roughly the same for GT TIT of 1216 °C and 1316 °C. Moreover, the pressure ratio difference between Case2 and Case3 are lower compared to Cycle 2 and Cycle 3 for all the GT TIT's which indicates that the efficiency (OPerational EXpenses- OPEX) vs CAPEX trade-off space is lower for Cycle 4.

Fig. 29 shows the trend of GT specific power, CC specific power, CC efficiency and pressure ratio for three GT TITs. The CC specific powers in Fig. 29 are normalised with 590.5, 680.5 and 763.6 kJ/kg for a GT TIT of 1216 °C, 1316 °C and 1416 °C respectively and the GT specific powers are normalised to 365.1, 422.3 and 482.7 kJ/kg respectively. This can be used to approximately estimate the expected thermal performance of integrating Cycle 4 with a commercial GT of defined pressure ratio and GT TIT. For an SGT5-4000F machine (Pressure ratio −17.2, GT TIT-1316 °C), integrating Cycle 4 as the bottoming cycle can offer the maximum efficiency of 59.0% whilst the maximum efficiency of 59.5% can be achieved at the pressure ratio of 24.6 (Table 11, case-1). This efficiency penalty might be higher for higher GT TITs owing to the diverging difference in pressure ratio between Case2 and Case3 as shown in Table 11.

5.5. Cascade Cycle 5

Fig. 30 illustrates the thermal Pareto front of Cycle 5 for three different GT TIT's. Examining Table 13, the maximum efficiency of Cycle 5 for a GT TIT of 1316 °C is 59.7% that was obtained at the pressure ratio of 20.0. This maximum efficiency for a GT TIT of 1316 °C is higher than Cycle 4 by 0.25% point and was obtained at an 18.5% lower pressure ratio than Cycle 4. Similarly, for a GT TIT of 1416 °C, the maximum efficiency of Cycle 5 is higher than Cycle 4 by 0.4% point which was obtained at a lower pressure ratio than Cycle 4 by ~21%. On the other hand, for Case3 the pressure drop is lower by 12.4% and 4.9% for a GT TI of 1316 °C and 1416 °C respectively. The difference in pressure ratio between Case2 and Case3 are 3.3, 2.1 and 4.8 for a GT TIT of 1216 °C, 1316 °C and 1416 °C respectively which is lower than cycler 4 for all the cases. This implies that despite the additional complexities involved with Cycle 5, this cycle might be a better candidate to integrate with higher GT TITs with lower pressure ratios. Although Cycle 5 can achieve ideal temperature gliding in both recuperators and flue gas heat exchangers, the maximum thermal efficiency occurs at the pressure ratio of 20.0 for a GT TIT of 1316 °C which is 16.5% higher than the equivalent steam-based SGT5-4000F pressure ratio. This indicates that in order to realise the maximum performance and cost reduction

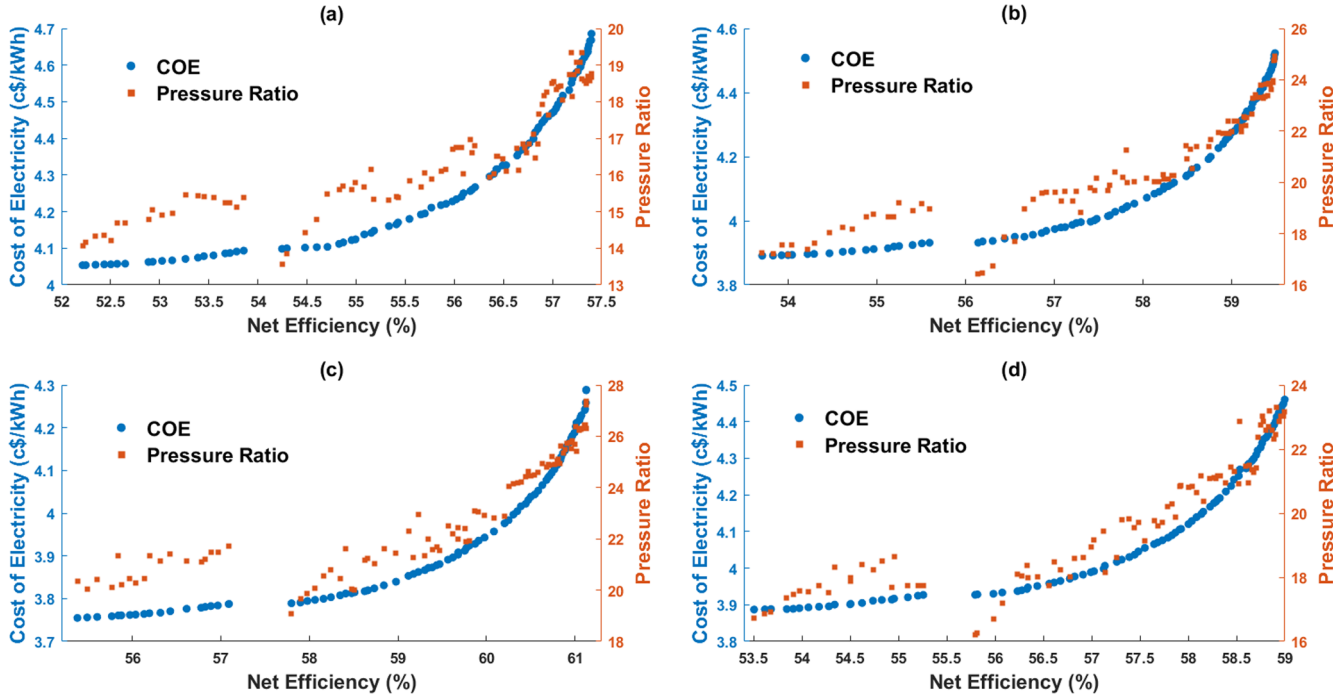

Fig. 28. Cycle 4 Cost Pareto fronts: (a) GT TIT-1216 °C, (b) GT TIT-1316 °C, (c) GT TIT-1416 °C, (d) GT TIT-1316 °C w/o intercooler.

Table 12
Cycle 4: Three cases from cost Pareto front for a GT TIT of 1216 °C, 1316 °C and 1416 °C.

GT TIT (°C)	Efficiency (%)			COE (c$/kWh)			Pressure Ratio			% Share Bot.cycle [d]		
	Case1[a]	Case2[b]	Case3[c]	Case1[a]	Case2[b]	Case3[c]	Case1[a]	Case2[b]	Case3[c]	Case1[a]	Case2[b]	Case3[c]
1216	57.4	53.1	57.3	4.7	4.1	4.6	18.8	14.9	19.1	31.9	29.7	31.5
1316	59.5	54.9	59.3	4.5	3.9	4.4	24.9	18.6	23.3	29.8	27.7	30.3
1416	61.1	56.3	61.0	4.3	3.8	4.2	27.4	21.1	25.7	29.6	27.0	30.2
1316[e]	59.0	54.5	58.9	4.5	3.9	4.4	23.2	18.0	22.6	29.9	27.6	30.0

[a] Maximum efficiency case.
[b] Minimum cost case.
[c] 95: 5 wt between efficiency and cost respectively in LINMAP.
[d] Power output share from the bottoming cycle.
[e] Without intercooler case.

potential of a sCO_2 cycle integrated with GT's, the whole plant has to be optimised. It is worth noting that the bottoming cycle energy share for a GT TIT of 1316 °C is higher than the equivalent steam Rankine cycle with SGT5-400F by 0.6% point (Table 13, Case-1). This indicates that this sCO_2 cycle can be attractive than steam cycles for higher GT TITs.

Fig. 31 illustrates the cost Pareto front of Cycle 5 and Table 14 shows the three cases from the cost Pareto front. As expected, the COE of Cycle 5 is higher by ~10% compared to Cycle 4 for a GT TIT of 1316 °C. The pressure ratio at the lowest COE is roughly the same as the pressure ratio which causes maximum GT specific power.

Fig. 32 can be used to estimate the maximum CC efficiency by integrating Cycle 5 with a particular GT and this curve is strictly valid for the considered modelling assumptions in this paper (Table 1). It is worth noting that the maximum CC occurs near to the maximum GT specific power condition.

5.6. Comparison between cascade cycles

The efficiency improvements from Cycle 2 to Cycle 5 in mainly caused by the trade-off between efficient exhaust heat recovery/recuperation and the bottoming cycle energy share. Since the exergy efficiency of the exhaust heat recovery and recuperation increases as the cycle complexity increases, the bottoming cycle energy share increases. In general, Cycle 3 achieves a higher efficiency at a lower pressure ratio compared with Cycle 2 while Cycle 4 surpasses Cycle 3 efficiency. The specific power of Cycle 4 and Cycle 5 are lower than Cycle 2 and Cycle 3 because of the increased back pressure by the additional heat exchangers in the flue gas path (Fig. 33). The optimal GT pressure ratio reduces from Cycle 2 to Cycle 5 for a given GT TIT, which indicates that the corresponding turbine exhaust temperature increases hence also the bottoming cycle energy share, to maximise the CC net efficiency, provided the cycle is flexible enough to maintain the stack temperature. Despite increasing the optimal GT pressure ratio for higher GT TITs, the bottoming cycle energy share of a sCO_2 cycle reduces as the GT TIT increases, similar to a steam bottoming cycle, as summarised in Tables 9, 11 and 13.

Examining Fig. 34, the COE of Cycle 2 at a maximum efficiency design is lower compared to Cycle 4 whilst it is higher than Cycle 3 by 1%. In general, Cycle 2 is not economically viable for higher GT TIT's (i.e. 1416 °C) as compared to Cycle 3. Even for lower GT TIT's, the COE of Cycle 3 is lower than Cycle 2 at higher cycle efficiencies. In addition, the higher efficiency of Cycle 3 was attained at relatively lower pressure ratios than Cycle 2, therefore, Cycle 3 can be integrated well for lower pressure ratio GTs. Cycle 2 may fit well with higher pressure ratio GTs (lower turbine exhaust temperature) for a small scale plant owing to the simple cycle of Cycle 2.

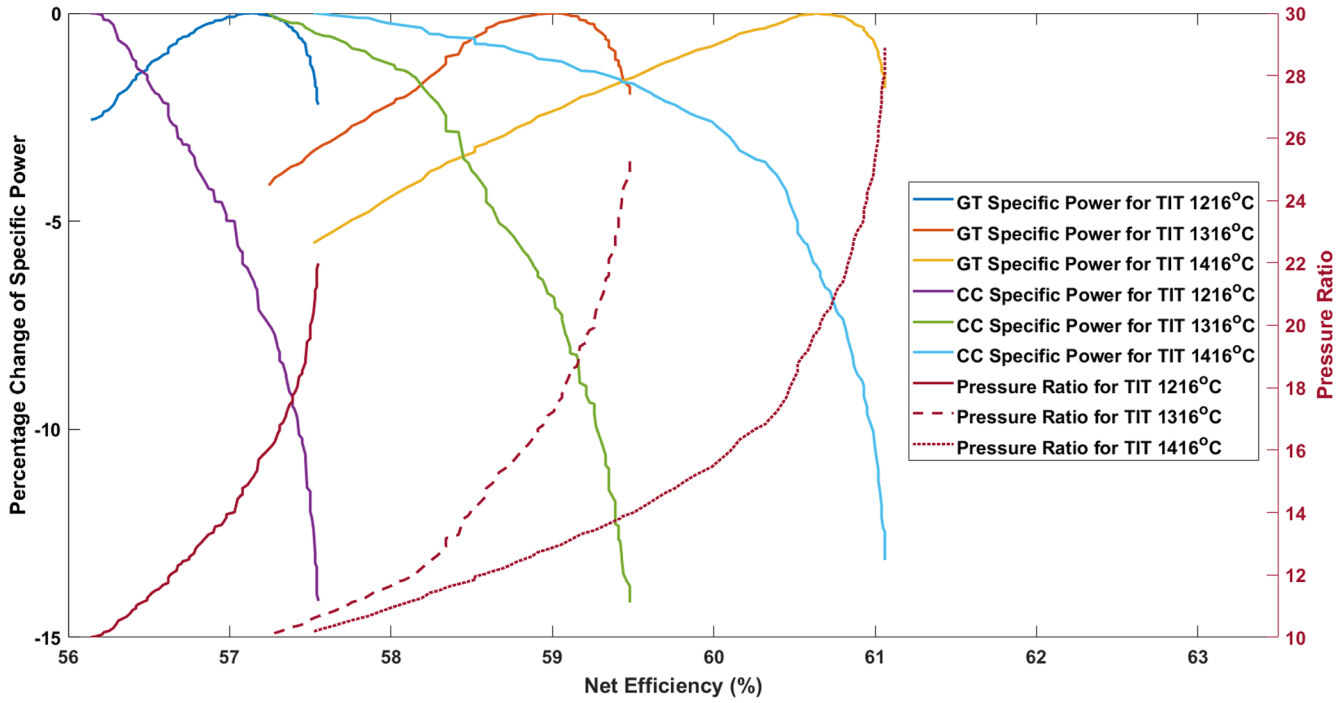

Fig. 29. Relationship between pressure ratio, efficiency and specific power for Cycle 4 for a GT TIT of 1216 °C, 1316 °C and 1416 °C.

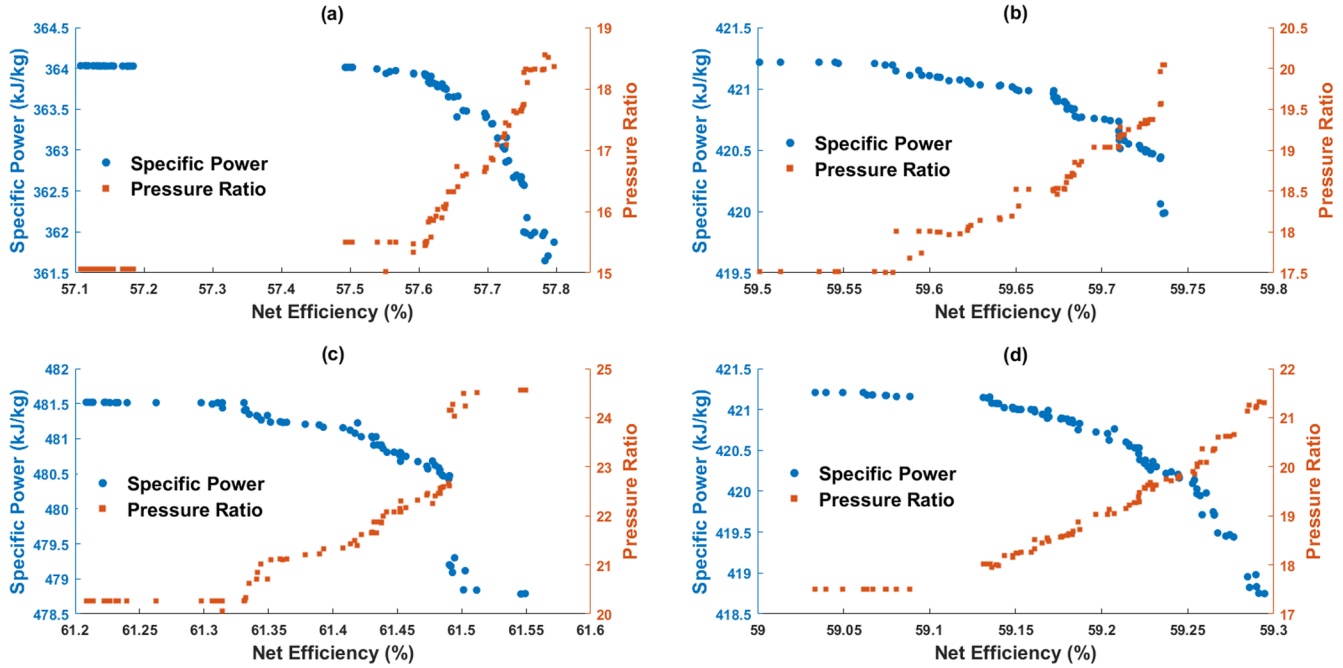

Fig. 30. Cycle 5 thermal Pareto fronts: (a) GT TIT-1216 °C, (b) GT TIT-1316 °C, (c) GT TIT-1416 °C, (d) GT TIT-1316 °C w/o intercooler.

The COE of Cycle 4 and Cycle 5 are higher than Cycle 3 for all the GT TITs. Although Cycle 4, and 5 can reach higher efficiencies than Cycle 3, the COE at the maximum efficiency point is higher than Cycle 3 which indicates that the increase in efficiency (reduction in OPEX) does not offset the increased CAPEX, therefore, these Cycles might not be economically attractive. This is evident from Fig. 34 where the COE of Cycle 3 is minimum for all the GT TITs studied at maximum efficiency point. It has to be noted that Cycle 4 and Cycle 5 can become an attractive option when the fuel cost is higher. However, in view of selecting an sCO_2 cycle for a commercially available GT for which the TIT and pressure ratio are fixed, Cycle 4 and Cycle 5 may be a good candidate for lower pressure ratio and higher temperature machines (higher turbine exhaust temperature) as the maximum efficiency of Cycle 4 and Cycle 5 is reached at a lower pressure ratio compared to Cycle 3. Nevertheless, an economic study has to be made as the COE of Cycle 4 and Cycle 5 is exponentially increasing near the maximum efficiency point (Fig. 34).

For a few commercial GTs, the GT firing temperature and the compressor pressure ratio may be not known from the open literature. For this case, the net power produced from a sCO2 cycle as bottoming cycle solution can be roughly predicted as a function of GT exhaust gas temperature. Fig. 35 shows that the bottoming cycle specific power varies almost linearly for the change in GT TET and Cycle 5 produces noticeably higher specific power than Cycle 3 and Cycle 4 for a higher

Table 13
Cycle 5: Three cases from thermal Pareto front for a GT TIT of 1216 °C, 1316 °C and 1416 °C.

GT TIT (°C)	Efficiency (%)			Specific Power (kJ/kg)			Pressure Ratio			% Share Bot.cycle [d]		
	Case1[a]	Case2[b]	Case3[c]	Case1[a]	Case2[b]	Case3[c]	Case1[a]	Case2[b]	Case3[c]	Case1[a]	Case2[b]	Case3[c]
1216	57.8	56.5	57.8	361.6	364.0	362.0	18.4	15.1	18.3	33.6	34.4	34.6
1316	59.7	57.7	59.7	420.0	421.2	420.4	20.0	17.5	19.6	32.7	32.8	33.3
1416	61.5	60.1	61.5	478.8	481.5	478.8	24.6	19.7	24.6	31.4	32.5	32.3
1316[e]	59.3	58.7	59.3	418.7	421.2	420.0	21.3	17.5	20.1	31.4	33.3	32.2

[a] Maximum efficiency case.
[b] Maximum GT specific power case.
[c] 85:15 wt between efficiency and specific power respectively in LINMAP.
[d] Power output share from the bottoming cycle.
[e] Without intercooler case.

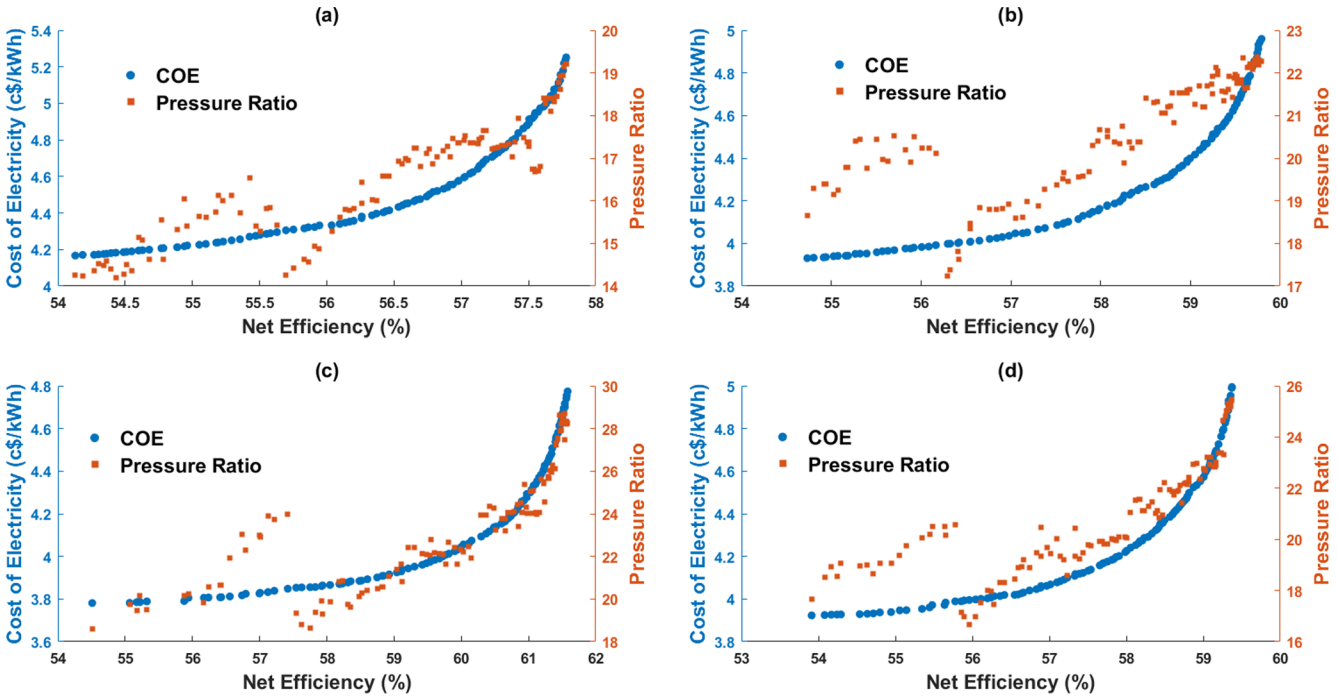

Fig. 31. Cycle 5 cost Pareto fronts: (a) GT TIT-1216 °C, (b) GT TIT-1316 °C, (c) GT TIT-1416 °C, (d) GT TIT-1316 °C w/o intercooler.

Table 14
Cycle 5: Three cases from cost Pareto front for a GT TIT of 1216 °C, 1316 °C and 1416 °C.

GT TIT (°C)	Efficiency (%)			COE (c$/kWh)			Pressure Ratio			% Share Bot.cycle [d]		
	Case1[a]	Case2[b]	Case3[c]	Case1[a]	Case2[b]	Case3[c]	Case1[a]	Case2[b]	Case3[c]	Case1[a]	Case2[b]	Case3[c]
1216	57.8	54.1	57.5	5.3	4.2	4.9	19.2	14.3	17.4	24.4	24.2	24.6
1316	59.8	54.7	59.5	5.0	3.9	4.7	22.3	18.7	21.7	31.4	27.6	31.3
1416	61.6	54.5	61.3	4.8	3.8	4.4	28.3	18.6	25.7	30.0	26.7	29.9
1316[e]	59.4	53.9	59.1	5.0	3.9	4.7	25.4	17.7	22.8	29.4	27.3	29.6

[a] Maximum efficiency case.
[b] Minimum cost case.
[c] 95: 5 wt between efficiency and cost respectively in LINMAP.
[d] Power output share from the bottoming cycle.
[e] Without intercooler case.

GT TETs. Net power produced from the bottoming cycle per unit mass flow of exhaust gas can be approximately estimated using Eq. (18),

$$NetPower_{sCO_2 cycle} = A * TET^2 + B * TET + C \quad (18)$$

where TET is the GT exhaust temperature in °C and the constants A, B and C are listed in Table 15 for different cycles with intercooler case. Also, the statistical coefficient of determination (R^2) value and the valid TET range of this equation are tabulated. It is worth noting that the influence of the second order terms is minimal.

6. Sensitivity analysis

Since this study focused on modelling the heavy duty SGT5-4000F machine, the applicability and the uncertainties of extending these

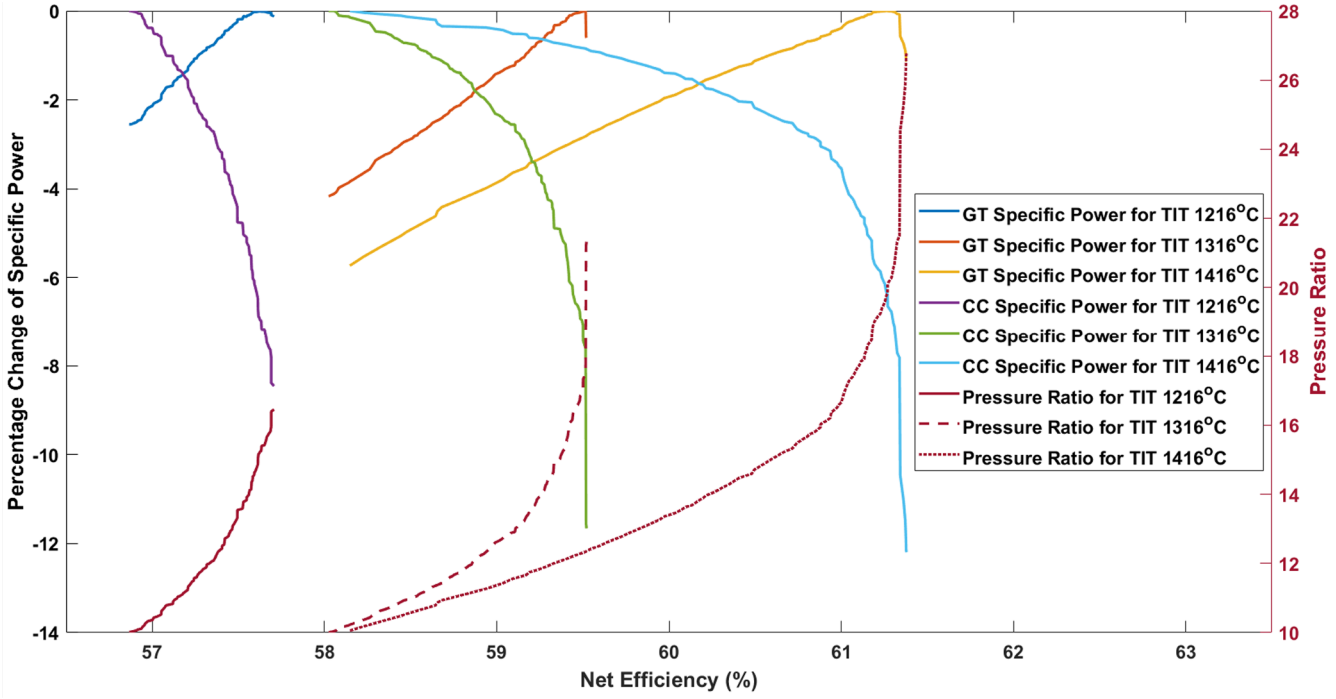

Fig. 32. Relationship between pressure ratio, efficiency and specific power for Cycle 5 for a GT TIT of 1216 °C, 1316 °C and 1416 °C.

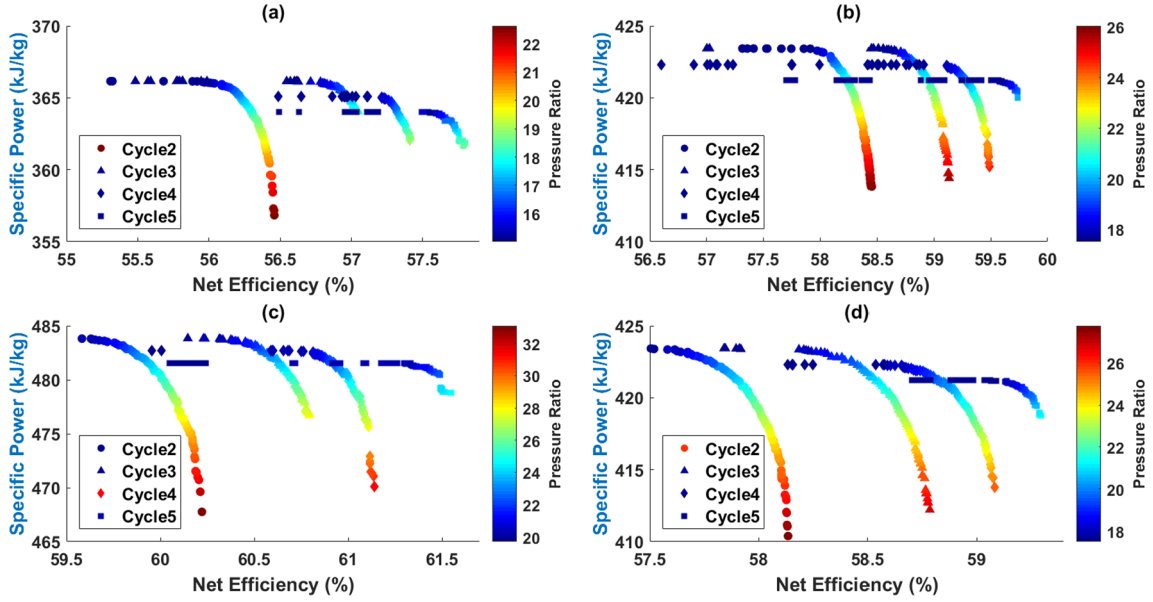

Fig. 33. Comparison of thermal Pareto fronts of Cycle 2, Cycle 3, Cycle 4 and Cycle 5: (a) GT TIT-1216 °C, (b) GT TIT-1316 °C, (c) GT TIT-1416 °C, and (d) GT TIT-1316 °C w/o intercooler.

results to different capacity GT's are discussed here. The air compressor polytropic efficiency and GT polytropic efficiency were kept constant during the optimization process and therefore the uncertainty of the optimal pressure ratio for a GT TIT of 1316 °C is analysed by performing a sensitivity study for Cycle 3 with intercooler. Moreover, the optimal pressure ratio is expected to change when the component cost functions change by changing the energy share of the bottoming cycle. Also, the fuel cost can change the pressure ratio which provides the minimum cost owing to the changes in the weight between CAPEX and OPEX in the calculation of COE. Agazzani and Massardo [42] indicated that the uncertainty of the cost function for GT components are ± 15%. Therefore, a sensitivity study is performed for the change in air compressor, combustor and GT cost variation by ± 20% to see the impact on the optimal pressure ratio of Cycle 3 with intercooler configuration. Since this study considered FOAK cost functions for sCO_2 cycle components the component cost can drop for Nth of a Kind (NOAK) plant. Therefore, a sensitivity study has also been undertaken for the variation in sCO_2 cycle components cost by −20% and −50%, however, it has to be noted that the uncertainty of sCO_2 cycle components is high.

From Fig. 36, it is evident that the variation in air compressor polytropic efficiency changes the thermal and cost Pareto fronts. The maximum specific power, maximum efficiency (Fig. 36(a)) and the corresponding pressure ratio (Fig. 36(c)) are reducing almost linearly as the compressor polytropic efficiency reduces. Table 16 shows three cases (1) maximum efficiency design (2) maximum (or minimum) specific power (or cost) and (3) 85% (or 95%) weight for efficiency and

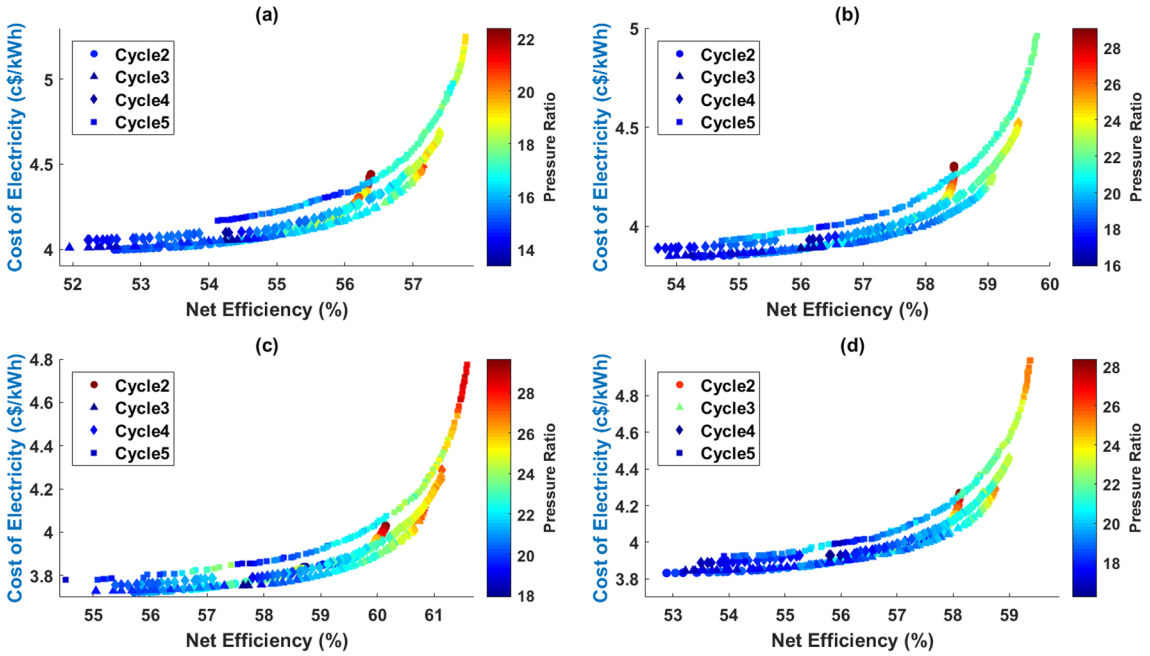

Fig. 34. Comparison of cost Pareto fronts of Cycle 2, Cycle 3, Cycle 4 and Cycle 5: (a) GT TIT-1216 °C, (b) GT TIT-1316 °C, (c) GT TIT-1416 °C, and (d) GT TIT-1316 °C w/o intercooler.

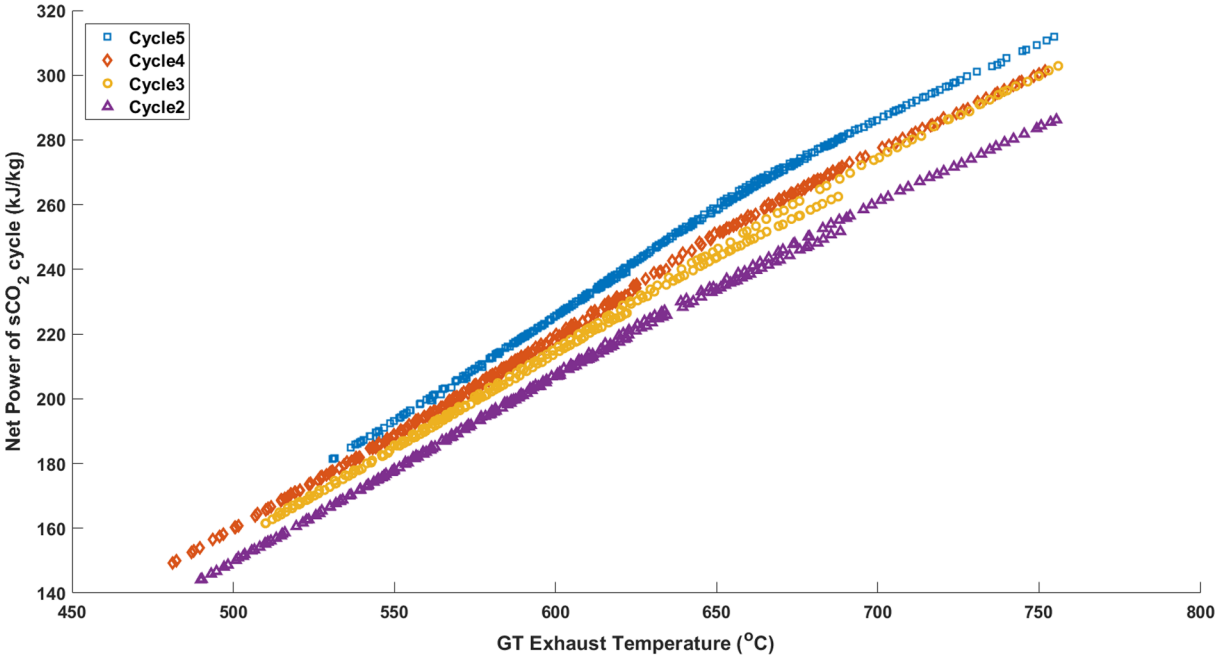

Fig. 35. Variation of net power of sCO_2 bottoming cycle for different GT outlet temperature.

Table 15
Constant values for estimating the sCO_2 bottoming cycle net power.

Cycle	A	B	C	R^2	TET Min °C	TET Max °C
Cycle 2	−0.000259	0.866439	−219.59280	0.9995	490	755
Cycle 3	−0.000104	0.716074	−177.28884	0.9990	510	755
Cycle 4	−0.000211	0.843716	−210.68713	0.9988	480	755
Cycle 5	−0.000611	1.390283	−387.67091	0.9989	530	730

15% (or 5%) weight to specific power (or COE). Table 16 indicates that the pressure ratio corresponding to maximum efficiency is lowered by ~18% for a 4% reduction in compressor polytropic efficiency. Although, the pressure ratio in the cost Pareto front is more scattered, the pressure ratio at which the COE is minimum is roughly the same for all the cases (Fig. 36(d), Table 16- Case2).

Fig. 37 depicts the thermal and cost Pareto fronts for three different GT polytropic efficiencies. Although the maximum efficiency and maximum GT specific power are reducing almost linearly as the GT polytropic efficiency reduces (Fig. 37(a), Table 17), the corresponding pressure ratio is highly non-linear. The COE at the maximum efficiency design is lower than the base case for a reduction of GT polytropic efficiency by 4% (Fig. 37(a)) whilst this is higher than the −2% case. The pressure ratio in the cost Pareto front is more scattered and also the pressure ratio at which the COE is minimum is not the same for all three cases (Fig. 37(d), Table 17- Case2). In general, the pressure ratio for

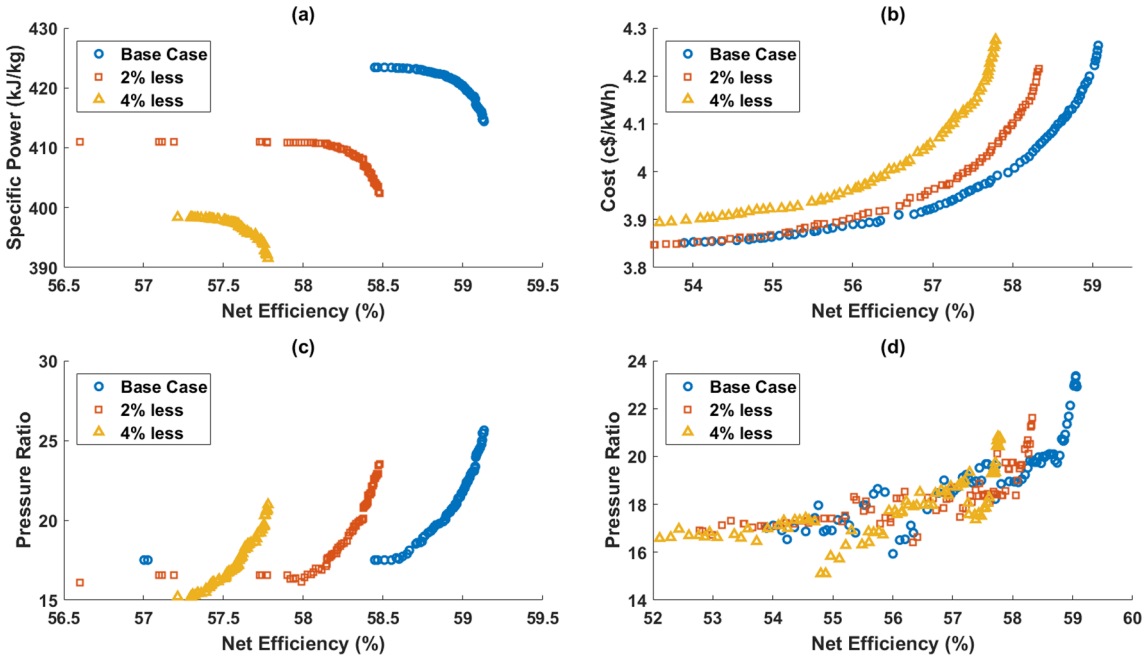

Fig. 36. Sensitivity study with compressor polytropic efficiency (a) Thermal Pareto front (b) Cost Pareto front (c) Pressure ratio of thermal Pareto front (d) Pressure ratio of cost Pareto front.

Table 16
Impact of change in compressor polytropic efficiency.

Case	Pareto Front	Efficiency (%)			Specific Power/COE (kJ/kg-s/c$/kWh)			Pressure Ratio		
		Case1	Case2	Case3	Case1	Case2	Case3	Case1	Case2	Case3
Base	Thermal	59.1	57.0	59.1	414.4	423.4	418.6	25.6	17.5	23.1
−2%[a]		−1.1%	2.4%	−1.2%	−2.9%	−2.9%	−2.5%	−8.2%	−8.2%	−12.9%
−4%[b]		−2.3%	0.4%	−2.3%	−5.5%	−5.9%	−5.7%	−18.2%	−13.2%	−16.8%
Base	Cost	59.1	53.9	59.0	4.3	3.9	4.2	22.9	17.0	22.9
−2%[a]		−1.3%	−2.1%	−1.3%	−1.1%	−0.2%	−1.5%	−5.6%	−0.6%	−10.7%
−4%[b]		−2.2%	−3.3%	−2.3%	0.3%	0.9%	−0.5%	−9.1%	−2.5%	−16.0%

[a] 2% lesser polytropic efficiency for air compressor.
[b] 4% lesser polytropic efficiency for air compressor.

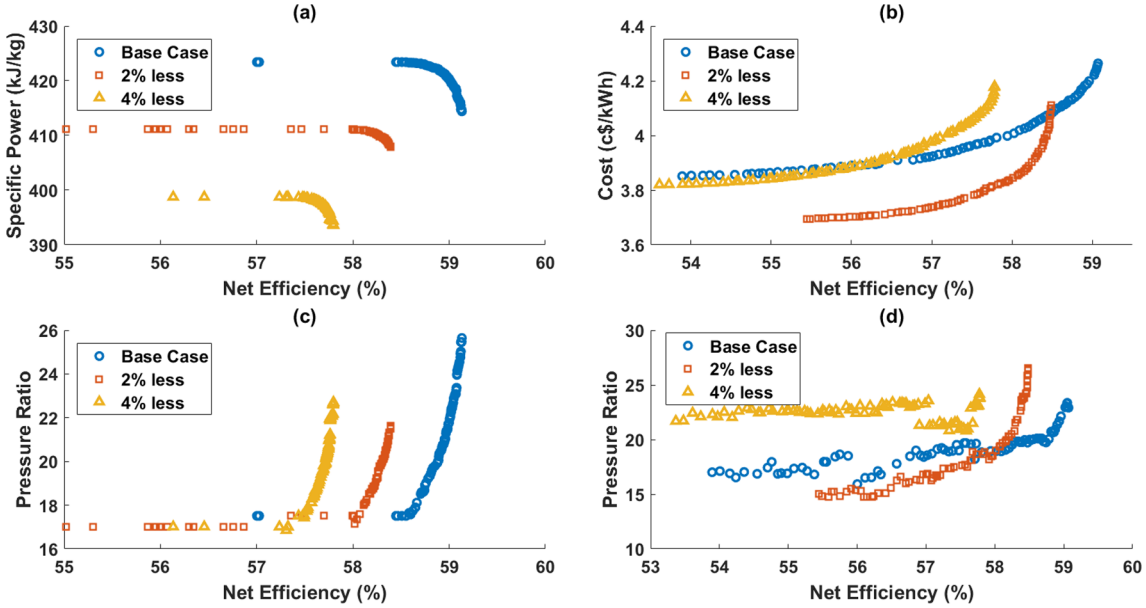

Fig. 37. Sensitivity study on gas turbine polytropic efficiency (a) Thermal Pareto front (b) Cost Pareto front (c) Pressure ratio of thermal Pareto front (d) Pressure ratio of cost Pareto front.

Table 17
Impact of change in gas turbine polytropic efficiency.

Case	Pareto Front	Efficiency (%)			Specific Power/COE (kJ/kg-s/c$/kWh)			Pressure Ratio		
		Case1	Case2	Case3	Case1	Case2	Case3	Case1	Case2	Case3
Base	Thermal	59.1	57.0	59.1	414.4	423.4	418.6	25.6	17.5	23.1
−2%[a]		−1.2%	−3.5%	−1.2%	−1.6%	−2.9%	−2.4%	−15.6%	−2.9%	−9.3%
−4%[b]		−2.3%	−1.5%	−2.2%	−5.0%	−5.8%	−5.3%	−11.4%	−2.9%	−10.8%
Base	Cost	59.1	53.9	59.0	4.3	3.9	4.2	22.9	17.0	22.9
−2%[a]		−1.0%	2.9%	−1.1%	−3.6%	−4.1%	−6.2%	15.9%	−11.6%	0.0%
−4%[b]		−2.2%	−1.0%	−2.2%	−2.0%	−0.8%	−2.6%	5.4%	27.5%	1.2%

[a] 2% lesser polytropic efficiency for a gas turbine.
[b] 4% lesser polytropic efficiency for a gas turbine

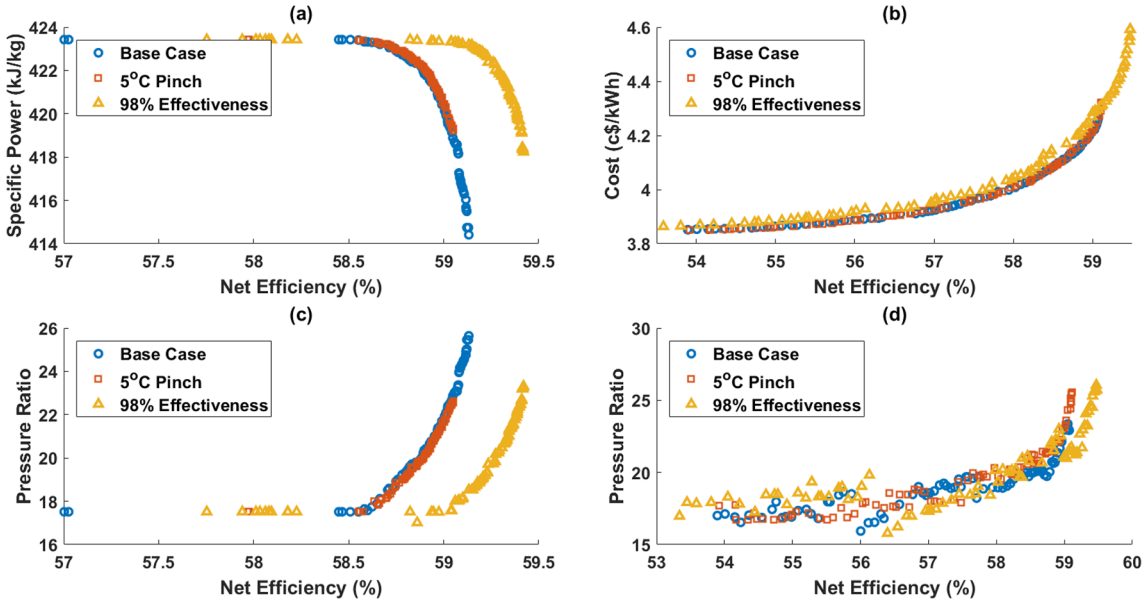

Fig. 38. Sensitivity study sCO_2 component performance change (a) Thermal Pareto front (b) Cost Pareto front (c) Pressure ratio of the thermal Pareto front (d) Pressure ratio of the cost Pareto front.

Table 18
Impact of change in sCO_2 component performance.

Case	Pareto Front	Efficiency (%)			Specific Power/COE (kJ/kg-s/c$/kWh)			Pressure Ratio		
		Case1	Case2	Case3	Case1	Case2	Case3	Case1	Case2	Case3
Base	Thermal	59.1	57.0	59.1	414.4	423.4	418.6	25.6	17.5	23.1
Case A[a]		0.5%	1.3%	0.5%	0.9%	0.0%	0.4%	−9.1%	0.0%	−5.7%
Case B[b]		−0.1%	1.7%	−0.1%	1.2%	0.0%	0.4%	−11.8%	0.0%	−5.5%
Base	Cost	59.1	53.9	59.0	4.3	3.9	4.2	22.9	17.0	22.9
Case A[a]		0.7%	−1.0%	0.4%	7.7%	0.3%	3.3%	12.4%	−0.2%	−5.4%
Case B[b]		0.1%	0.0%	0.0%	1.4%	0.0%	0.0%	11.6%	4.0%	1.4%

[a] 98% Recuperator effectiveness.
[b] 5 °C pinch.

maximum thermal efficiency is significantly changed (non-linearly) when the GT polytropic efficiency is changing.

Fig. 38 compares the thermal and cost Pareto fronts of the base case with two different sCO_2 cycle performance parameter; (A) 98% effectiveness (Thermoflex method) for the sCO_2 cycle recuperators (B) 5 °C minimum pinch constraint for the heat exchangers. Examining Fig. 38, Case B doesn't notably influence the performance of the cycle compared to the base case. For Case A, on the other hand, the maximum efficiency increased by ~0.7% in the cost Pareto front. It is worth noting from Fig. 38(b) that the cost Pareto front for Case B is shifted up by a lightly from the base case in the cost coordinates along with an exponential increase in cost near the maximum efficiency design (7.7% increment). In general, the Case A and Case B have little impact on the pressure ratio at which maximum efficiency/specific power or minimum cost is obtained (Table 18).

Fig. 39 and Table 19 illustrates the impact of the cost Pareto fronts for the changes in component costs by a fixed factor. Four cases were simulated (A) the total GT components cost was reduced by 80% (B) the total GT components cost was reduced by 120% (C) the total sCO_2 components cost was reduced by 80% (D) the total sCO_2 components cost was reduced by 50%. The maximum efficiency didn't change for all the four scenarios which reinforce the robustness toward converging to the globally optimum solution. Examining Fig. 39 (c, d), it is clear that increasing the GT component cost reduces the pressure ratio and vice

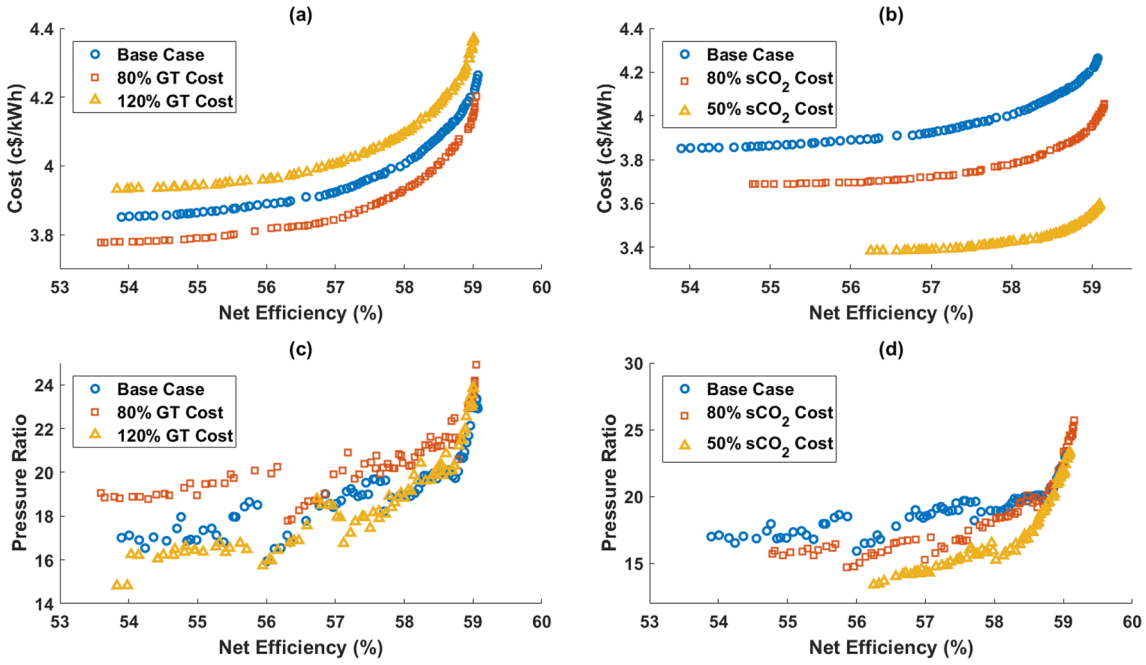

Fig. 39. Sensitivity study: Impact of component cost (a) Change of GT cost (b) Change of sCO_2 cost (c) Pressure ratio of change of GT cost (d) Pressure ratio of change of sCO_2 cost.

Table 19
Impact in Cycle performance for changes in component cost.

Case	Efficiency (%)			COE (c$/kWh)			Pressure Ratio		
	Case1	Case2	Case3	Case1	Case2	Case3	Case1	Case2	Case3
Base	59.1	53.9	59.0	4.3	3.9	4.2	22.9	17.0	22.9
Case A[a]	0.0%	−0.6%	−0.1%	−1.4%	−1.9%	−2.4%	8.7%	12.0%	0.5%
Case B[b]	−0.1%	−0.1%	−0.2%	2.5%	2.1%	1.3%	4.1%	−12.9%	−4.2%
Case C[c]	0.1%	1.6%	0.1%	−13.5%	5.3%	−5.4%	12.1%	−7.6%	5.4%
Case D[d]	0.0%	4.4%	0.0%	−20.7%	−6.6%	−15.4%	1.9%	−21.2%	−0.5%

[a] 80% of GT components cost.
[b] 120% of GT components cost.
[c] 80% of sCO_2 components cost.
[d] 50% of sCO_2 components cost.

versa and reducing the sCO_2 cycle component cost reduces the pressure ratio. The CC efficiency corresponding to a minimum cost is highly dependent on the component cost functions (CAPEX) and fuel cost (OPEX). Reducing the sCO_2 cycle component cost increases the efficiency corresponding to the minimum cost design in the cost Pareto front and it is evident in Fig. 39 (d). The pressure ratio for changes in component cost functions does not significantly change the pressure ratio at which maximum efficiency can be obtained.

7. Conclusions

This study considered five sCO_2 cascade cycles in lieu of a conventional steam Rankine cycle in a CCPP with an industrial SGT5-4000F class heavy-duty GT and analysed using multi-objective optimisation with regard to thermal and economic performance. To the authors knowledge, for the first time this optimisation included the GT pressure ratio as a design variable, finding that this has significant impact on the cycle performance. Simulations were performed for several GT TITs to explore the change in performance for different sCO_2 cycle configurations. The maximum CC efficiency with a sCO_2 bottoming cycle occurs at a higher GT pressure ratio compared to equivalent conventional steam Rankine cycle. Therefore a sCO_2 cycle integrated with a commercial GT does not offer its maximum efficiency and maximum cost reduction unless the GT pressure ratio is proximate to the optimal value reported in this work. For example, integrating Cycle 4 with an SGT5-4000F machine without optimising the GT pressure ratio penalises the maximum efficiency by 0.5% point.

At maximum CC efficiency the optimal GT pressure ratio increases with GT firing temperature increases, which indicates that the energy share from the bottoming cycle is reduced. The pressure ratio that corresponds to maximum CC efficiency of a complex sCO_2 cycle configuration (i.e. Cycle 5, Cycle 4 and Cycle 3) is lower than simple configurations (i.e. Cycle 2, Cycle 1). Furthermore, the difference in pressure ratio between maximum CC efficiency and maximum GT specific power is highest for Cycle 2 and reduces as the degrees of freedom of the sCO_2 bottoming cycle increase (i.e. Cycle 3, Cycle 4 and Cycle 5). Therefore complex cycles are good for industrial heavy-duty machines that typically have a lower pressure ratio, to maximise the combined cycle efficiency. This paper gives performance maps for four sCO_2 Cycles, which helps in estimating the CC efficiency and specific power for any given GT pressure ratio and TIT, though extrapolation of these maps requires attention. Also, empirical correlation between net power from each sCO_2 Cycle and the hot flue gas temperature was proposed, which can also be used for WHR applications.

It was also observed that for all the GT TITs and for the sCO_2 configurations studied the GT pressure ratio corresponding to the lower

COE design is proximate to the GT pressure ratio of the maximum GT specific power case. The efficiencies at the lowest COE is lower than a steam based cycle, nevertheless, that is highly sensitive to the component cost functions (CAPEX) and fuel cost/efficiency (OPEX), therefore, NOAK cost functions may yield higher efficiencies at lower COE design.

The novel sCO_2 cycle proposed yields a 1.4% point higher net efficiency than a conventional three pressure steam Rankine cycle integrated with the SGT5-4000F machine; this cycle offers an ideal temperature glide in the heat exchangers. The COE of this Cycle is higher than Cycle 4, nonetheless, the pressure ratio that corresponds to maximum efficiency occurs at a lower pressure ratio than Cycle 4. Therefore, this cycle can be attractive for high-temperature sensible heat sources owing to its large degree of flexibility that helps in accommodating the large variation in C_p to a lower stack temperature. In Cycle 5, the recuperators and exhaust heat exchangers were arranged in parallel and connected via splitter/mixers in order to control the mass flow split, additional recuperators and exhaust heat exchangers can be connected, though the improvement in performance might be negligible in comparison to the added cost.

Acknowledgement

This work was supported by the Biomass and Fossil Fuel Research Alliance (BF2RA), United Kingdom under grant 26-sCO2 for efficient power generation and the Engineering and Physical Sciences Research Council, United Kingdom (EPSRC Grant No: EP/N029429/1). The author also would like to thank the Sir Richard Stapley Educational Trust, United Kingdom for providing financial support for the year 2018–19. Data underlying this paper can be accessed at https://doi.org/10.17862/cranfield.rd.9783818.

References

[1] Guidance 2050 Pathways. GovUk 2013. https://www.gov.uk/guidance/2050-pathways-analysis [accessed December 12, 2018].
[2] Herzog HJ, Rubin ES, Rochelle GT. Comment on “reassessing the efficiency penalty from carbon capture in coal-fired power plants”. Environ Sci Technol 2016;50:6112–3. https://doi.org/10.1021/acs.est.6b00169.
[3] Persichilli M, Kacludis A, Zdankiewicz E, Held T. Supercritical CO_2 power cycle developments and commercialization: why sCO_2 can displace steam steam. power-gen india cent. Asia 2012:1–15.
[4] Dostal V, Driscoll MJ, Hejzlar P. A supercritical carbon dioxide cycle for next generation nuclear reactors; 2004. doi:MIT-ANP-TR-100.
[5] Turchi CS, Ma Z, Neises T, Michael W. Thermodynamic study of advanced supercritical carbon dioxide power cycles for high performance concentrating solar power systems. Proc. ASME 2012 6th Int. Conf. Energy Sustain.. 2012.
[6] Steven W, Tom C, Edward P, Tom L, Gary R. Summary of the Sandia supercritical CO_2 development program. Int. SCO2 Power Cycle Symp.. 2011.
[7] Park SH, Kim JY, Yoon MK, Rhim DR, Yeom CS. Thermodynamic and economic investigation of coal-fired power plant combined with various supercritical CO_2 Brayton power cycle. Appl Therm Eng 2018;130:611–23. https://doi.org/10.1016/j.applthermaleng.2017.10.145.
[8] Thimsen D, Weitzel P. Challenges in designing fuel-fired sCO_2 heaters for closed sCO_2 Brayton cycle power plants. 5th Int Symp. – Supercrit. CO2 Power Cycles. 2016.
[9] Allam R, Martin S, Forrest B, Fetvedt J, Lu X, Freed D, et al. Demonstration of the Allam cycle: an update on the development status of a high efficiency supercritical carbon dioxide power process employing full carbon capture. Energy Procedia 2017;114(The Author(s)):5948–66. https://doi.org/10.1016/j.egypro.2017.03.1731.
[10] Crespi F, Gavagnin G, Sánchez D, Martínez GS. Supercritical carbon dioxide cycles for power generation: a review. Appl Energy 2017;195:152–83. https://doi.org/10.1016/j.apenergy.2017.02.048.
[11] Zhao Y, Zhao L, Wang B, Zhang S, Chi J, Xiao Y. Thermodynamic analysis of a novel dual expansion coal-fueled direct-fired supercritical carbon dioxide power cycle. Appl Energy 2018;217:480–95. https://doi.org/10.1016/j.apenergy.2018.02.088.
[12] Heo JY, Kim MS, Baik S, Bae SJ, Lee JI. Thermodynamic study of supercritical CO_2 Brayton cycle using an isothermal compressor. Appl Energy 2017;206:1118–30. https://doi.org/10.1016/j.apenergy.2017.08.081.
[13] Wang X, Dai Y. Exergoeconomic analysis of utilizing the transcritical CO_2 cycle and the ORC for a recompression supercritical CO_2 cycle waste heat recovery: a comparative study. Appl Energy 2016;170:193–207. https://doi.org/10.1016/j.apenergy.2016.02.112.
[14] Baik YJ, Kim M, Chang KC, Kim SJ. Power-based performance comparison between carbon dioxide and R125 transcritical cycles for a low-grade heat source. Appl Energy 2011;88:892–8. https://doi.org/10.1016/j.apenergy.2010.08.029.
[15] Weiland NT, Dennis RA, Ames R, Lawson S, Strakey P. Fundamentals and applications of supercritical carbon dioxide (sCO_2) based power cycles-Fossil energy. Elsevier Ltd; 2017.
[16] Khadse A, Blanchette L, Kapat J, Vasu S, Ahmed K. Optimization of supercritical CO_2 Brayton cycle for simple cycle gas turbines exhaust heat recovery using genetic algorithm. ASME Turbo Expo. 2017. p. 1–8.
[17] Khadse A, Blanchette L, Kapat J, Vasu S, Ahmed K. Optimization of supercritical CO_2 Brayton cycle for simple cycle gas turbines exhaust heat recovery using genetic algorithm. Energy Resour Technol 2018;140:1–8. https://doi.org/10.1115/1.4039446.
[18] Marchionni M, Bianchi G, Tassou SA. Techno-economic assessment of Joule-Brayton cycle architectures for heat to power conversion from high-grade heat sources using CO_2 in the supercritical state. Energy 2018;148:1140–52. https://doi.org/10.1016/j.energy.2018.02.005.
[19] Kimzey G. Development of a Brayton bottoming cycle using supercritical carbon dioxide as the working fluid; 2012.
[20] Cho SK, Kim M, Baik S, Ahn Y. Investigation of the bottoming cycle for high efficiency combined cycle gas turbine system with supercritical carbon dioxide. Proc. ASME Turbo Expo 2015 Turbine Tech. Conf. Expo.,. 2015. p. 1–12.
[21] Wright SA, Davidson CS, Scammell WO. Thermo-economic analysis of four sCO_2 waste heat recovery power systems. 5th Int Symp – Supercrit CO2 Power Cycles. 2016. p. 1–16.
[22] Held TJ. Supercritical CO_2 cycles for gas turbine combined cycle power plants. Power Gen Int 2015.
[23] Huck P, Freund S, Lehar M, Peter M. Performance comparison of supercritical CO_2 versus steam bottoming cycles for gas turbine combined cycle applications. 5th Int Symp - SCO2 Power Cycles. 2016. p. 1–14.
[24] Davidson BJ, Keeley KR. The thermodynamics of practical combined cycles. Proc IMechE Conf Comb Cycle Gas Turbines. 1991. p. 28–50.
[25] Cerri G. Parametric analysis of combined gas-steam cycles. J Eng Gas Turbines Power 1987;109.
[26] Horlock JH. Advanced gas turbine cycles; 2003.
[27] Najjar YSH, Ismail MS. Optimum pressure ratios for different gas turbine cycles. High Temp Technol 1990;8:283–9. https://doi.org/10.1080/02619180.1990.11753494.
[28] Thermoflow. Tflow16 Update Letter 2006. https://www.thermoflow.com/UpdateLetters/TF16_UPDATE_LETTER.html [accessed June 20, 2018].
[29] Zhao Q, Mecheri M, Neveux T, Privat R, Jaubert JN. Selection of a proper equation of state for the modeling of a supercritical CO_2 Brayton cycle: consequences on the process design. Ind Eng Chem Res 2017;56:6841–53. https://doi.org/10.1021/acs.iecr.7b00917.
[30] Lemmon EW, Bell IH, Huber ML, McLinden MO. NIST Standard Reference Database 23: Reference Fluid Thermodynamic and Transport Properties-REFPROP, Version 10.0. 2010. doi:http://doi.org/10.18434/T4JS3C.
[31] Heatric. Compact Heat Exchange. Meggitt Smart Eng Extrem Environ 2018:1–5.
[32] Nellis G, Klein S. Heat transfer. Cambridge Univ. Press; 2009. p. 1143.
[33] Avval HB, Ahmadi P, Ghaffarizadeh AR, Saidi MH. Thermo-economic-environmental multiobjective optimization of a gas turbine power plant with preheater using evolutionary algorithm. Int J Energy Res 2010. https://doi.org/10.1002/er.1696.
[34] Sharma S, Rangaiah GP, Cheah KS. Multi-objective optimization using MS Excel with an application to design of a falling-film evaporator system. Food Bioprod Process 2011;90:123–34. https://doi.org/10.1016/j.fbp.2011.02.005.
[35] Rangaiah GP. Multi-Objective optimization techniques and applications in chemical engineering. vol. 1; 2009. doi:http://doi.org/10.1007/0-387-28356-0_10.
[36] Ahmadi MH, Hosseinzade H, Sayyaadi H, Mohammadi AH, Kimiaghalam F. Application of the multi-objective optimization method for designing a powered Stirling heat engine: Design with maximized power, thermal efficiency and minimized pressure loss. Renew Energy 2013;60:313–22. https://doi.org/10.1016/j.renene.2013.05.005.
[37] Wang Z, Rangaiah GP. Application and analysis of methods for selecting an optimal solution from the pareto-optimal front obtained by multiobjective optimization. Ind Eng Chem Res 2016;56:560–74. https://doi.org/10.1021/acs.iecr.6b03453.
[38] Ho CK, Carlson M, Garg P, Kumar P. Technoeconomic analysis of alternative solarized sCO_2 Brayton cycle configurations. J Sol Energy Eng 2016;138:051008https://doi.org/10.1115/1.4033573.
[39] ESDU 92013: Selection and costing of heat exchangers; 1994.
[40] Marchionni M, Bianchi G, Tsamos KM, Tassou SA. Techno-economic comparison of different cycle architectures for high temperature waste heat to power conversion systems using CO_2 in supercritical phase. Energy Procedia 2017;123:305–12.
[41] Zada KR, Kim R, Wildberger A, Schalansky CP. Analysis of supercritical CO_2 Brayton cycle recuperative heat exchanger size and capital cost with variation of layout design. 6th Int Symp. - Supercrit. CO2 Power Cycles. 2018.
[42] Agazzani A, Massardo AF. A tool for thermoeconomic analysis and optimization of gas, steam, and combined plants. Eng Gas Turbines Power 1997;1. https://doi.org/10.1115/1.2817069.
[43] McMahon T. Inflation Rate Calculator 2018. https://inflationdata.com/Inflation/Inflation_Calculators/Inflation_Rate_Calculator.asp [accessed December 12, 2018].
[44] Valero A, Lozano MA, Serra L, Tsatsaronis G, Pisa J, Frangopoulos C, et al. CGAM problem: definition and conventional solution. Energy 1994;19:279–86. https://doi.org/10.1016/0360-5442(94)90112-0.
[45] Horlock JH. The optimum pressure ratio for a combined cycle gas turbine plant. Proc Instn Mech Eng 1995;209:259–64.